On the Improvement of Vibration Mitigation and Energy Harvesting Using Electromagnetic Vibration Absorber-Inerter: Exact H_2 Optimization

Eshagh Farzaneh Joubaneh
Department of Mechanical Engineering,
Central Michigan University,
Mount Pleasant, MI 48858
e-mails: farza1e@cmich.edu;
eshaghfarzaneh@gmail.com

Oumar Rafiou Barry[1]
Department of Mechanical Engineering,
Virginia Tech,
Blacksburg, VA 24060
e-mail: obarry@vt.edu

Electromagnetic resonant shunt tuned mass damper-inerter (ERS-TMDI) has recently been developed for dual-functional vibration suppression and energy harvesting. However, energy harvesting and vibration mitigation are conflicting objectives, thus rendering the multi-objectives optimization problem a very challenging task. In this paper, we aim at solving the design trade-off between these two objectives by proposing alternative configurations and finding the model with the best performance for both vibration suppression and energy harvesting. Three novel configurations are presented and are compared with the conventional ERS-TMDI. In the first two configurations, the primary structure and the absorber are only coupled through the spring. Both inerter and electromagnetic devices are connected to the ground in the first configuration, whereas only the inerter is connected to the ground in the second configuration. The third configuration is inspired by the recently developed three-element vibration-inerter (TEVAI), but in this case an electromagnetic device is sandwiched in between the primary structure and the absorber. Closed-form expressions are presented for optimum vibration mitigation and energy harvesting performances using H_2 criteria for both ground and force excitations. The obtained explicit expressions are validated using MATLAB optimization toolbox. Simulation examples reveal that the first configuration performs the best, whereas the second performs the worst in terms of both vibration mitigation and energy harvesting. It is also demonstrated that replacing the series RLC with a parallel circuit can improve or degrade the vibration mitigation performance, but it constantly enhances the energy harvesting performance in all four models. [DOI: 10.1115/1.4044303]

Keywords: ERS-TMDI, vibration suppression, energy harvesting, inerter, RLC, H_2

1 Introduction

Many engineering structures and components such as bridges, power lines, buildings, airplanes, and cars are usually plagued with unwanted vibrations, making them prone to fatigue failure. The most common passive strategy for mitigating these unwanted vibrations is to attach tuned mass damper (TMD), namely, vibration absorbers, to the main structure such that significant kinetic energy from the primary structure is transferred to the attached vibration absorber [1–3]. Numerous researchers have employed various optimization techniques such as the fixed point, H_2, and H_∞ methods to optimize the design parameters of TMDs, thereby improving the performance of TMDs [4]. Ormondroyd and Hartog [4] and Brock [5] are among the first investigators to present explicit expressions for optimal TMD stiffness and damping properties using the "fixed point" theory. Their proposed closed-form expressions are widely employed in TMD design for vibration suppression.

Despite their wide practical usage, TMDs suffer from detuning problems, which is partly due to uncertainties and variations to the dynamic properties of the primary structure over time [6–8]. Various strategies have been explored to address this detuning problem. One such technique is to exploit the benefit of stiffness and damping nonlinearities for widening the operational frequency range [9,10]. Other strategies for enhancing TMD performance and robustness include attaching multiple TMDs in parallel [11–13], or in series configurations [14], and/or increasing the mass of TMD [8]. The larger the mass of the vibration absorber, the more effective an optimally designed linear TMD is for suppressing vibration of the primary structure and more robust to detuning effects [8,15]. However, this advantage comes at a huge cost of an increase in total weight of the overall vibration absorber device.

To address the aforementioned trade-off, TMDs can be coupled with an inerter device [16], which is a mass amplification device with negligible physical weight. An inerter is a two-terminal flywheel mechanical device, which provides a force proportional to the relative acceleration of its two terminals. When coupled with TMD, an inerter increases the inertia of the TMD without increasing the overall weight of the controlled structure [8]. The earliest inerter implementations consist of a rack-pinion or ball-screws mechanism to drive the rotating flywheel. The performance of such flywheel-based inerters is therefore dependent on the number of gears and gearing ratio used to drive the flywheel [8,17]. The concept of coupling vibration absorber or isolators with an inerter is not new. For many years, researchers have employed inerters for improving vibration suppression in cars [18–20], railways [21,22], and many civil engineering structures [23–25]. It has been demonstrated that

[1]Corresponding author.

Contributed by the Technical Committee on Vibration and Sound of ASME for publication in the JOURNAL OF VIBRATION AND ACOUSTICS. Manuscript received October 13, 2018; final manuscript received July 12, 2019; published online July 22, 2019. Assoc. Editor: Alper Erturk.

an optimum designed configuration of a tuned mass damper-inerter (TMDI) can perform much better than an optimum designed classical TMD in terms of vibration mitigation of the primary structure [8,17]. This kind of passive control device works as a two-terminal device in which their two terminals are free to move relative to each other, producing a force proportional to the relative acceleration of its terminals. Two different configurations of inerters such as rack-pinion [22] or ball screw [26] have been widely used in passive vibration controller in order to convert the relative linear motion to rotational motion by means of an object such as flywheel with a large moment of inertia. Based on the size of flywheel and gearing ratio, the inerter can produce an apparent mass hundred times larger than the physical mass [27,28].

Numerous investigators have also incorporated electromagnetic and/or piezoelectric transducers in TMDs for the potential of simultaneously harvesting energy and suppressing vibration [29,30]. The transducer selection depends on specific applications. Piezoelectric transducers are limited to small-scale energy harvesting applications, while electromagnetic motors are suitable for large-scale energy harvester applications such as civil structures and shock absorbers [31]. The general idea for simultaneous energy harvesting and vibration control is to replace or to complement the mechanical damping element by an electromagnetic device so that all the energy is not dissipated through the device as heat, but rather the energy is recovered electrically and then stored in batteries. The generated energy can then be used to achieve self-powered semi-active/active vibration control or/and to power wireless sensors for structural health monitoring [29,32–34]. However, it is well documented in the literature that energy harvesting and vibration mitigation are two conflicting objectives [35,36]. For instance, the closed-form expressions for maximum energy harvesting and vibration suppression presented in Ref. [35] clearly show an inverse proportional relationship. This design trade-off is obviously dependent on the way the vibration absorber is connected to the primary structure. To relax this design trade-off, a novel configuration was proposed in Ref. [23]. The proposed configuration named energy harvesting enabled tuned mass-damper-inerter (EH-TMDI) couples the classical TMD with a grounded inerter connected in series with a standard electromagnetic device and the mass of the vibration absorber. It should be noted that the electromagnetic device is only connected to the inerter and the absorber instead of being sandwiched in between the primary structure and the TMD.

Inspired by the EH-TMDI configuration presented in Ref. [23], the three-element vibration-inerter (TEVAI) in Ref. [37], and the electromagnetic shunted with an RLC circuit in Ref. [36], we seek to further develop an EH-TMDI with improved vibration control and energy harvesting capabilities using various configurations. The proposed configurations include (i) a grounded electromagnetic resonant shunt tuned mass damper-inerter (GERS-TMDI) in which the electromagnetic transducer is grounded on one side and connected to the vibration absorber on the other; (ii) three-element electromagnetic resonant shunt tuned mass damper-inerter with series connection (TE-ERS-TMDI-S), in which the electromagnetic transducer is connected in series to the grounded inerter on one side and to the absorber on the other side; (iii) three-element electromagnetic resonant shunt tuned mass damper-inerter with parallel connection (TE-ERS-TMDI-P), in which the electromagnetic transducer is sandwiched in between the absorber and the primary structure; and (iv) the conventional ERS-TMDI [36,38,39]. The primary structure is subjected to both ground and force excitations. The GERS-TMDI and the series and parallel TE-ERS-TMDIs configurations are presented for the first time in this paper. The difference between the EH-TMDI in Ref. [23] and our proposed GERS-TMDI is that here both the inertance and the electromagnetic transducer are connected in parallel, whereas, they are connected in series in Ref. [23]. Also in Ref. [23], no explicit expressions were found for energy harvesting and vibration suppressions. Different from the proposed GERS-TMDI, the configuration in Ref. [36] had the electromagnetic device sandwiched in between the primary structure and the TMD, making the relaxation of the design trade-off between energy harvesting and vibration suppression impossible to achieve.

Also, the recently published TEVAI configuration [37] is different since it is only a mechanical vibration absorber, whereas the proposed series and parallel TE-ERS-TMDIs are electromechanical absorbers capable of simultaneously harvesting energy and suppressing vibration. Also, none of the works in the literature examines parallel circuit configuration. Here, for the first time, (i) we derived closed-form expressions of optimum energy harvesting and vibration suppression of three novel configurations under both harmonic and ground excitations and (ii) we examined both parallel and series RLC circuit configurations. The optimum expressions were analytically obtained using H_2 optimization and then validated using MATLAB optimization toolbox. Simulation examples are provided to compare the performance of the different configurations and the results show that the GERS-TMDI design possesses the best performance in comparison with the other models. Parametric studies are then carried out to examine the effect of mass and inertance ratios on the performance of the GERS-TMDI model. Numerical simulations are also presented to compare the influence of series and parallel RLC circuits on all models.

2 Mathematical Modeling

A schematic of the rack-and-pinion-flywheel-based inerter is depicted in Fig. 1. Such an inerter consists of rack and pinion gearing system connected to a flywheel. The rack-and-pinion transforms the translational kinetic energy associated with the relative motion of the device terminals into a rotational kinetic energy of a small physical flywheel mass. All four ERS-TMDI configurations depicted in Fig. 2 employ a rack-and-pinion-flywheel-based inerter.

The primary structure m_s with a linear spring k_s and damping coefficient c_s is coupled with the ERS-TMDI of mass m_T and stiffness k_T. The inertance of the system, denoted by b, is grounded at one end and connected to the absorber mass at the other end. The resistance, inductance, and capacitance of the electrical circuit are denoted by R, L, and C, respectively. The electromagnetic transducer is installed in four different configurations: (a) electromagnetic transducer is grounded on one side and connected to the TMD on the other; (b) electromagnetic transducer is connected to the base structure via an extra spring k_e on one side and to the absorber on the other; (c) electromagnetic transducer is sandwiched in between the absorber and the inerter; and (d) electromagnetic absorber is sandwiched in between the primary structure and the absorber [36,38,39].

3 H_2 Optimization for ERS-TMDI Configurations

In this section, explicit expressions for the optimum parameters of the four ERS-TMDI models are presented using the H_2 norm criteria.

3.1 GERS-TMDI Configuration. The governing equations of motion of the coupled system presented in Fig. 2(*a*) with a

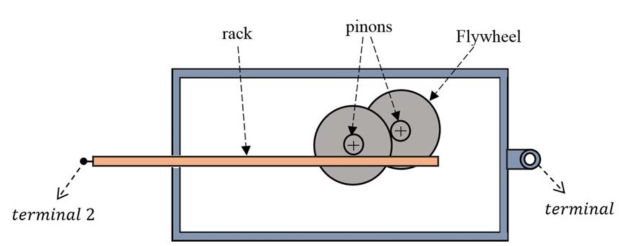

Fig. 1 Schematic of inerter with rack and pinion mechanism

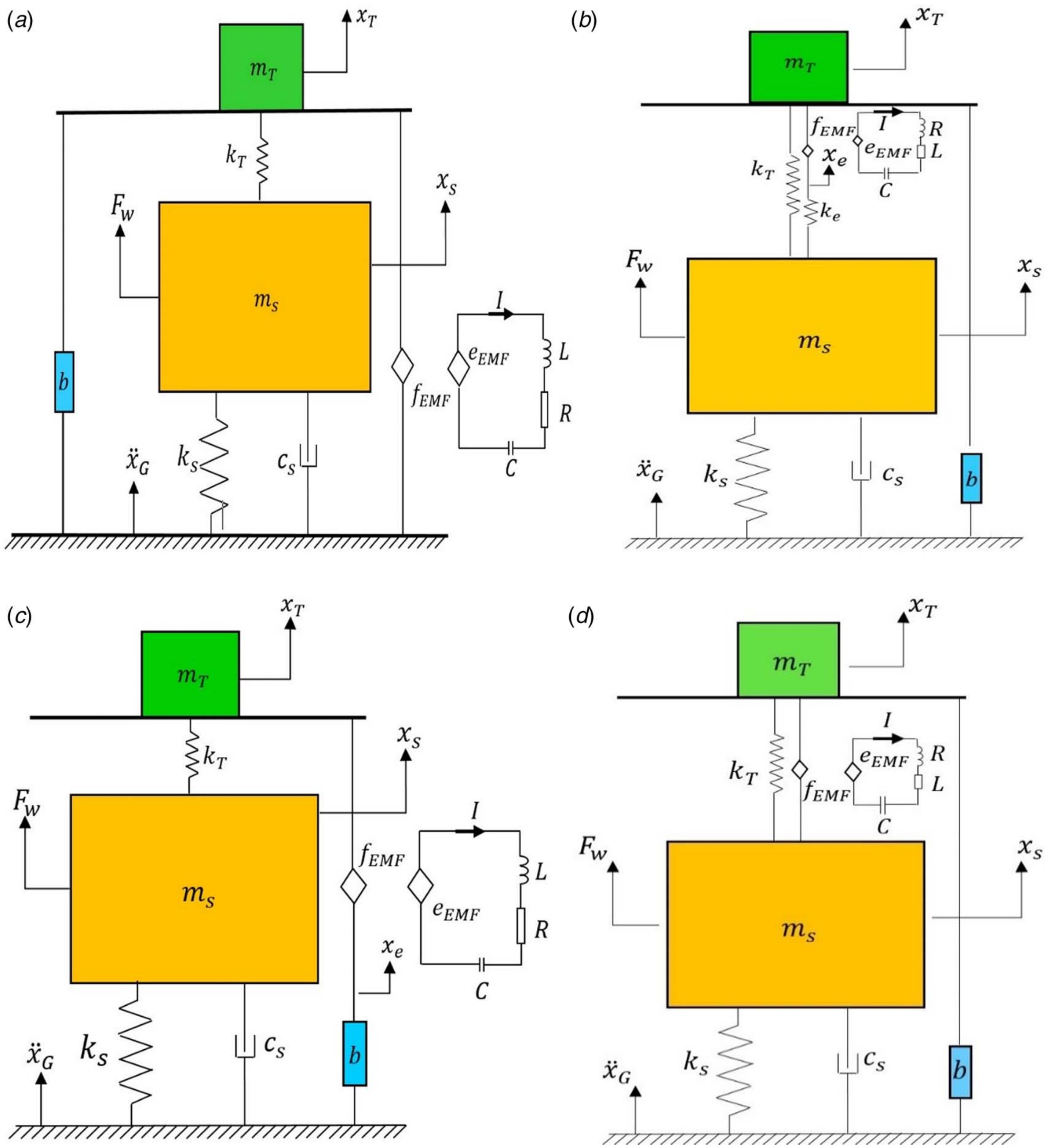

Fig. 2 Schematic diagram of host structure with ERS-TMDI absorber: (*a*) GERS-TMDI, (*b*) TE-ERS-TMDI-P, (*c*) TE-ERS-TMDI-S, and (*d*) ERS-TMDI

series RLC circuit subjected to force (F_w) and ground ($\ddot{x}_g$) excitations can be obtained as

$$m_s\ddot{x}_s + c_s\dot{x}_s + k_s x_s - k_T(x_T - x_s) = F_w - m_s\ddot{x}_g \tag{1a}$$

$$(m_T + b)\ddot{x}_T + k_T(x_T - x_s) + k_f I = -(m_T + b)\ddot{x}_g \tag{1b}$$

$$-k_v\dot{x}_T + RI + L\dot{I} + \frac{1}{C}\int I dt = 0 \tag{1c}$$

Applying Laplace transform into Eq. (1) and considering the primary structure undamped ($c_s = 0$), the equations of motion become

$$(m_s s^2 + k_s + k_T)X_s - k_T X_T = F_w - m_s s^2 X_s \tag{2a}$$

$$-k_T X_s + ((m_T + b)s^2 + k_T)X_T + k_f I = -(m_T + b)s^2 X_g \tag{2b}$$

$$-k_v s X_T + RI + LIs + \frac{I}{CS} = 0 \tag{2c}$$

Equation (2c) can be written as

$$I = \frac{k_s}{k_f} q_1(X_T) \tag{3}$$

where

$$q_1 = \frac{f_t^2 \mu\mu_k (j\alpha)^2}{(j\alpha)^2 + 2\zeta_e f_e (j\alpha) + f_e^2} \tag{4}$$

Substituting Eq. (3) into Eq. (2) and dividing them by k_s, the nondimensional equations of motion reduce to

$$[(j\alpha)^2 + (1 + f_t^2\mu)]X_s - f_t^2\mu X_T = \frac{F_w}{K_s} - \frac{\ddot{X}_g}{\omega_s^2} \tag{5a}$$

$$-f_t^2\mu X_s + [\psi(j\alpha)^2\mu + f_t^2\mu + q_1]X_s = -\mu\psi\frac{\ddot{X}_g}{\omega_s^2} \tag{5b}$$

The parameters used in the dynamic of the system are defined in Table 1.

Here, k_v and k_f are the voltage and force constants of the electromagnetic transducer, respectively.

3.1.1 Force Excitation. Following Ref. [35], the optimum parameters of f_T, f_e, μ_k, and ζ_e to minimize the vibrations of the primary structure (x_s) caused by the force excitation, F_w/k_s can be obtained as follows:

$$PI = \frac{1}{2\pi}\int_{-\infty}^{\infty}\left|\frac{X_s(j\alpha)}{F_w/K_s}\right|^2 d\alpha \tag{6}$$

where $(X_s(j\alpha)/\ K_s)/F_w$ is the normalized transfer function and is given as

Table 1 Definitions of parameters used in the dynamic equations

Data	Definition
ω	Excitation frequency
$\omega_s = \sqrt{k_s/m_s}$	Natural frequency of the primary structure
$\omega_T = \sqrt{k_T/m_T}$	Natural frequency of the tuned mass
$\omega_e = 1/\sqrt{LC}$	Resonant natural frequency of the circuit
$\mu = m_T/m_s$	Mass ratio of the tuned mass to the primary structure (mass ratio)
$\delta = b/m_T$	Mass ratio of the inertance to the tuned mass (inertance ratio)
$\psi = \delta + 1$	
$f_T = \omega_T/\omega_s$	Mechanical tuning ratio
$f_e = \omega_e/\omega_s$	Electrical tuning ratio
$\alpha = \omega/\omega_s$	Normalized frequency
$\zeta_e = R/(2L\omega_e)$	Electrical damping ratio
$\mu_k = k_f k_v/k_T L$	Electromagnetic mechanical coupling coefficient
k_v	Voltage constant of the transducer
k_f	Force constant of the transducer
$K_r = \frac{k_e}{k_s}$	Relative stiffness

$$\frac{X_s(j\alpha)\ K_s}{F_w} = \frac{B_4(j\alpha)^4 + B_3(j\alpha)^3 + B_2(j\alpha)^2 + B_1(j\alpha) + B_0}{A_6(j\alpha)^6 + A_5(j\alpha)^5 + A_4(j\alpha)^4 + A_3(j\alpha)^3 + A_2(j\alpha)^2 + A_1(j\alpha) + A_0} \tag{7}$$

where

$$\left\{\begin{array}{c} A_6 = \psi \\ A_5 = 2f_e\psi\zeta_e \\ A_4 = \psi + f_t^2 + f_t^2\mu_k + f_e^2\psi + f_t^2\mu\psi \\ A_3 = 2f_e\psi\zeta_e + 2f_e f_t^2\zeta_e + 2f_e f_t^2\mu\psi\zeta_e \\ A_2 = f_t^2 + f_t^2\mu_k + f_e^2\psi + f_e^2 f_t^2 + f_t^4\mu\mu_k + f_e^2 f_t^2\mu\psi \\ A_1 = 2f_e f_t^2\zeta_e \\ A_0 = f_e^2 f_t^2 \end{array}\right. \qquad \left\{\begin{array}{c} B_4 = \psi \\ B_3 = 2f_e\psi\zeta_e \\ B_2 = f_t^2 + f_t^2\mu_k + f_e^2\psi \\ B_1 = 2f_e f_t^2\zeta_e \\ B_0 = f_e^2 f_t^2 \end{array}\right. \tag{8}$$

Applying the residue theorem [40] into Eq. (6), the performance index (PI) can be obtained as

$$\begin{aligned} PI = {} & (f_e^4 f_t^4\mu\psi + f_e^4 f_t^4 - 2f_e^4 f_t^2\psi + f_e^4\psi^2 + f_e^2 f_t^6\mu\mu_k - 2f_e^2 f_t^4\mu_k + 4f_e^2 f_t^4\zeta_e^2 - 2f_e^2 f_t^4 + 4f_e^2 f_t^2\mu\psi^2\zeta_e^2 - 2f_e^2 f_t^2\mu\psi^2 + 2f_e^2 f_t^2\mu_k\psi - 8f_e^2 f_t^2\psi\zeta_e^2 \\ & + 4f_e^2 f_t^2\psi + 4f_e^2\psi^2\zeta_e^2 - 2f_e^2\psi^2 + f_t^4\mu^2\psi^2 - 2f_t^4\mu\mu_k\psi - f_t^4\mu\psi + f_t^4\mu_k^2 + 2f_t^4\mu_k + f_t^4 + 2f_t^2\mu\psi^2 - 2f_t^2\mu_k\psi - 2f_t^2\psi + \psi^2)/(4f_e f_t^6\mu\mu_k\zeta_e) \end{aligned} \tag{9}$$

Setting the derivation of PI with respect to design parameters to zero, we obtain

$$\frac{\partial PI}{\partial f_t} = 0, \quad \frac{\partial PI}{\partial \mu_k} = 0, \quad \frac{\partial PI}{\partial f_e} = 0, \quad \frac{\partial PI}{\partial \zeta_e} = 0 \tag{10}$$

The four gradients' equations can be then obtained as

$$\begin{aligned} \frac{\partial PI}{\partial f_t} = {} & (4f_e^2 f_t^4 + 8f_e^2 f_t^2\mu\psi^2 + 12f_e^2\psi^2 - 16f_e^2 f_t^2\psi)\zeta_e^2 + (f_e^4 f_t^4\mu\psi + f_e^4 f_t^4 - 4f_e^4 f_t^2\psi + 3f_e^4\psi^2 - 2f_e^2 f_t^4\mu_k - 2f_e^2 f_t^4 - 4f_e^2 f_t^2\mu\psi^2 \\ & + 4f_e^2 f_t^2\mu_k\psi + 8f_e^2 f_t^2\psi - 6f_e^2\psi^2 + f_t^4\mu^2\psi^2 - 2f_t^4\mu\mu_k\psi - f_t^4\mu\psi + f_t^4\mu_k^2 + 2f_t^4\mu_k + f_t^4 + 4f_t^2\mu\psi^2 - 4f_t^2\mu_k\psi - 4f_t^2\psi + 3\psi^2) = 0 \end{aligned} \tag{11a}$$

$$\begin{aligned} \frac{\partial PI}{\partial \mu_k} = {} & +(4f_e^2 f_t^2\mu\psi^2 - 8f_e^2 f_t^2\psi + 4f_e^2\psi^2)\zeta_e^2(f_e^4 f_t^4\mu\psi + f_e^4 f_t^4 - 2f_e^4 f_t^2\psi + f_e^4\psi^2 - 2f_e^2 f_t^4 - 2f_e^2 f_t^2\mu\psi^2 + 4f_e^2 f_t^2\psi - 2f_e^2\psi^2 + f_t^4\mu^2\psi^2 \\ & - f_t^4\mu\psi - f_t^4\mu_k^2 + f_t^4 + 2f_t^2\mu\psi^2 - 2f_t^2\psi + \psi^2) = 0 \end{aligned} \tag{11b}$$

$$\begin{aligned} \frac{\partial PI}{\partial f_e} = {} & (4f_e^2 f_t^4 - 8f_e^2 f_t^2\psi + 4f_e^2 f_t^2\mu\psi^2 + 4f_e^2\psi^2)\zeta_e^2 + (3f_e^4 f_t^4\mu\psi + 3f_e^4 f_t^4 - 6f_e^4 f_t^2\psi + 3f_e^4\psi^2 + f_e^2 f_t^6\mu\mu_k - 2f_e^2 f_t^4\mu_k - 2f_e^2 f_t^4 - 2f_e^2 f_t^2\mu\psi^2 \\ & + 2f_e^2 f_t^2\mu_k\psi + 4f_e^2 f_t^2\psi - 2f_e^2\psi^2 - f_t^4\mu^2\psi^2 + 2f_t^4\mu\mu_k\psi + f_t^4\mu\psi - f_t^4\mu_k^2 - 2f_t^4\mu_k - f_t^4 - 2f_t^2\mu\psi^2 + 2f_t^2\mu_k\psi + 2f_t^2\psi - \psi^2) = 0 \end{aligned} \tag{11c}$$

$$\frac{\partial PI}{\partial \zeta_e} = (-4f_e^2 f_t^4 - 4f_e^2 f_t^2 \mu\psi^2 - 4f_e^2\psi^2 + 8f_e^2 f_t^2\psi)\zeta_e^2 + (f_e^4 f_t^4 \mu\psi + f_e^4 f_t^4 - 2f_e^4 f_t^2\psi + f_e^4\psi^2 + f_e^2 f_t^6 \mu\mu_k - 2f_e^2 f_t^4\mu_k - 2f_e^2 f_t^4 - 2f_e^2 f_t^2\mu\psi^2 + 2f_e^2 f_t^2\mu_k\psi + 4f_e^2 f_t^2\psi - 2f_e^2\psi^2 + f_t^4\mu^2\psi^2 - 2f_t^4\mu\mu_k\psi - f_t^4\mu\psi + f_t^4\mu_k^2 + 2f_t^4\mu_k + ft^4 + 2f_t^2\ \mu\psi^2 - 2f_t^2\mu_k\psi - 2f_t^2\psi + \psi^2) = 0 \tag{11d}$$

Using the four gradient equations above (Eq. (11)) with some algebraic manipulations, one can obtain an expression in terms of just one variable, in this case f_t, by following the seven steps described below

(1) Express ζ_e^2 in terms of other parameters using Eq. (11*b*) as $\zeta_e^2 = f(f_t, f_e, \mu_k, \mu, \psi)$.
(2) The obtained equation from Step (1) can be substituted in the other three equations (i.e., 11*a*, 11*c*, and 11*d*). The resulting equations are in terms of parameters f_t, f_e, μ_k, μ, and ψ and can be expressed as

$$4f_e^4 f_t^8\mu\psi + 4f_e^4 f_t^8 + 6f_e^4 f_t^6\mu^2\psi^3 - 6f_e^4 f_t^6\mu\psi^2 - 24f_e^4 f_t^6\psi - 8f_e^4 f_t^4\mu\psi^3 + 48f_e^4 f_t^4\psi^2 + 10f_e^4 f_t^2\mu\psi^4 - 40f_e^4 f_t^2\psi^3 + 12f_e^4\psi^4 + 2f_e^2 f_t^{10}\mu\mu_k + 4f_e^2 f_t^8\mu^2\mu_k\psi^2 - 8f_e^2 f_t^8\mu\mu_k\psi - 8f_e^2 f_t^8\mu_k - 8f_e^2 f_t^8 - 6f_e^2 f_t^6\mu\mu_k\psi^2 - 24f_e^2 f_t^6\mu\psi^2 + 36f_e^2 f_t^6\mu_k\psi + 48f_e^2 f_t^6\psi - 16f_e^2 f_t^4\mu^2\psi^4 + 16f_e^2 f_t^4\mu\mu_k\psi^3 + 64f_e^2 f_t^4\mu\psi^3 - 48f_e^2 f_t^4\mu_k\psi^2 - 96f_e^2 f_t^4\psi^2 - 40f_e^2 f_t^2\mu\psi^4 + 20f_e^2 f_t^2\mu_k\psi^3 + 80f_e^2 f_t^2\psi^3 - 24f_e^2\psi^4 + 4f_t^8\mu^2\psi^2 - 8f_t^8\mu\mu_k\psi - 4f_t^8\mu\psi + 4f_t^8\mu_k^2 + 8f_t^8\mu_k + 4f_t^8 + 6f_t^6\mu^3\psi^4 - 12f_t^6\mu^2\mu_k\psi^3 - 18f_t^6\mu^2\psi^3 + 6f_t^6\mu\mu_k^2\psi^2 + 36f_t^6\mu\mu_k\psi^2 + 30f_t^6\mu\psi^2 - 12f_t^6\mu_k^2\psi - 36f_t^6\mu_k\psi - 24f_t^6\psi + 24f_t^4\mu^2\psi^4 - 32f_t^4\mu\mu_k\psi^3 - 56f_t^4\mu\psi^3 + 8f_t^4\mu_k^2\psi^2 + 48f_t^4\mu_k\psi^2 + 48f_t^4\psi^2 + 30f_t^2\mu\psi^4 - 20f_t^2\mu_k\psi^3 - 40f_t^2\psi^3 + 12\psi^4 = 0 \tag{12a}$$

$$(f_t^6\mu - 2f_t^4)\mu_k + 4f_t^2\psi - 2f_t^4 - 2\psi^2 + 2f_e^2 f_t^4 + 2f_e^2\psi^2 + 2f_t^2\mu_k\psi - 4f_e^2 f_t^2\psi - 2f_t^2\mu\psi^2 + 2f_e^2 f_t^4\mu\psi = 0 \tag{12b}$$

$$2f_t^4\mu_k - 4f_t^2\psi + 2f_t^4 + 2\psi^2 - 4f_e^2 f_t^4 + 2f_e^4 f_t^4 - 4f_e^2\psi^2 + 2f_e^4\psi^2 - 2f_t^4\mu\psi - 2f_t^2\mu_k\psi - 2f_e^2 f_t^4\mu_k + 8f_e^2 f_t^2\psi - 4f_e^4 f_t^2\psi + 4f_t^2\mu\psi^2 + 2f_t^4\mu^2\psi^2 - 4f_e^2 f_t^2\mu\psi^2 - 2f_t^4\mu\mu_k\psi + f_e^2 f_t^6\mu\mu_k + 2f_e^4 f_t^4\mu\psi + 2f_e^2 f_t^2\mu_k\psi = 0 \tag{12c}$$

(3) Similar to step 1, write μ_k in terms of the rest of the parameters using Eq. (12*b*) such as $\mu_k = f(f_t, f_e, \mu, \psi)$.
(4) The obtained equation from step 3 can be substituted into the other equations (Eqs. (12*a*) and (12*c*)) and can be written as

$$2f_e^4 f_t^{10}\mu^3\psi^3 - 2f_e^4\ f_t^{10}\mu^2\psi^2 - 8f_e^4 f_t^{10}\mu\psi - 8f_e^4 f_t^{10} - 12f_e^4 f_t^8\mu^2\psi^3 + 16f_e^4 f_t^8\mu\psi^2 + 32f_e^4 f_t^8\psi - 2f_e^4 f_t^6\mu^2\psi^4 - 8f_e^4 f_t^6\mu\psi^3 - 48f_e^4 f_t^6\psi^2 + 32f_e^4 f_t^4\psi^3 - 8f_e^4 f_t^2\psi^4 + 4f_e^2 f_t^{12}\mu - 4f_e^2 f_t^{10}\mu^2\psi^2 - 24f_e^2 f_t^{10}\mu\psi + 8f_e^2 f_t^{10} - 16f_e^2 f_t^8\mu^{3\psi^4} + 16f_e^2 f_t^8\mu^2\psi^3 + 80f_e^2 ft^{8\mu\psi^2} - 8f_e^2 f_t^8\psi + 28f_e^2 f_t^6\mu^2\psi^4 - 104f_e^2 f_t^6\mu\psi^3 - 48f_e^2 f_t^6\psi^2 - 8f_e^2 f_t^4\mu^2\psi^5 + 44f_e^2 f_t^4\mu\psi^4 + 112f_e^2 f_t^4\psi^3 - 88f_e^2\ f_t^2\psi^4 + 24f_e^2\psi^5 - 4f_t^{12}\mu^3\psi^2 + 4f_t^{12}\mu^2\psi - 4f_t^{12}\mu - 6f_t^{10}\mu^4\psi^4 + 18f_t^{10}\mu^3\psi^3 - 14f_t^{10}\mu^2\psi^2 + 24f_t^{10}\mu\psi + 8f_t^8\mu^2\psi^3 - 48f_t^8\mu\psi^2 - 24f_t^8\psi - 6f_t^6\mu^2\psi^4 + 16f_t^6\mu\psi^3 + 96f_t^6\psi^2 - 8f_t^4\mu^2\psi^5 + 36f_t^4\mu\psi^4 - 144f_t^4\psi^3 - 24f_t^2\mu\psi^5 + 96f_t^2\psi^4 - 24\psi^5 = 0 \tag{13a}$$

$$f_e^2(-f_t^4 + f_t^2\mu\psi^2 + 2f_t^2\psi - \psi^2) + f_t^4\mu^2\psi^2 - f_t^4\mu\psi + f_t^4 - 2f_t^2\psi + \psi^2 = 0 \tag{13b}$$

(5) Write parameter f_e in terms of the other parameters by means of Eq. (13*b*) such as $f_e = f(f_t, \mu, \psi)$.
(6) Substitute the obtained equation from Step (5) in Eq. (13*a*) and the resultant equation can be written in terms of the optimum parameter f_t and the two other design parameters μ and ψ as follows

$$(f_t^6\mu^3\psi^3 - 3f_t^6\mu^2\psi^2 + f_t^6\mu\psi - 4f_t^6 - 2f_t^4\mu^2\psi^3 + 2f_t^4\mu\psi^2 + 12f_t^4\psi - 3f_t^2\mu\psi^3 - 12f_t^2\psi^2 + 4\psi^3) = 0 \tag{14}$$

(7) Solve the above third-order polynomial equation (Eq. (14)) to obtain the optimum parameter f_t, which can be written as

$$f_{t_{\text{opt}}} = \sqrt{-\frac{A^*}{2}} \tag{15}$$

where

$$A^* = A + 3^{\frac{1}{2}}\left(Ai - \frac{Bi}{9Ag^2}\right) + \frac{4\psi h}{3g} + \frac{B}{9Ag^2} \tag{16a}$$

$$r = \sqrt{-3\mu^3(68\mu^3\psi^3 + 849\mu^2\psi^2 - 3360\mu\psi + 256)} \tag{16b}$$

$$g = \mu\psi - 3\mu^2\psi^2 + \mu^3\psi^3 - 4 \tag{16c}$$

$$h = -\mu^2\psi^2 + \mu\psi + 6 \tag{16d}$$

$$A = \left(\frac{r\psi^3}{9g^2} - \frac{8\psi^3 h^3}{27g^3} - \frac{2\psi^3}{g} - \frac{\psi^3(\mu\psi + 4)(h)}{(g)^2}\right)^{\frac{1}{3}} \tag{16e}$$

$$B = \mu\psi^3(13\mu^3\psi^3 + \mu^2\psi^2 - 143\mu\psi + 48) \tag{16f}$$

The other three optimum parameters f_e, μ_k, ζ_e can be obtained by using the equations obtained from steps 5, 3, and 1, respectively, and can be expressed as

$$f_{e_{\text{opt}}} = \sqrt{-\frac{f_{t_{\text{opt}}}^4\mu^2\psi^2 - f_{t_{\text{opt}}}^4\mu\psi + f_{t_{\text{opt}}}^4 - 2f_{t_{\text{opt}}}^2\psi + \psi^2}{-f_{t_{\text{opt}}}^4 + \mu f_{t_{\text{opt}}}^2\psi^2 + 2f_{t_{\text{opt}}}^2\psi - \psi^2}} \tag{17}$$

$$\mu_{k_{\text{opt}}} = -\frac{2\mu f_{e_{\text{opt}}}^2 f_{t_{\text{opt}}}^4 \psi + 2f_{e_{\text{opt}}}^2 f_{t_{\text{opt}}}^4 - 4f_{e_{\text{opt}}}^2 f_{t_{\text{opt}}}^2 \psi + 2f_{e_{\text{opt}}}^2 \psi^2 - 2f_{t_{\text{opt}}}^4 - 2\mu f_{t_{\text{opt}}}^2 \psi^2 + 4f_{t_{\text{opt}}}^2 \psi - 2\psi^2}{\mu f_{t_{\text{opt}}}^6 - 2f_{t_{\text{opt}}}^4 + 2\psi f_{t_{\text{opt}}}^2} \tag{18}$$

$$\begin{aligned}\zeta_{e_{\text{opt}}} = ((&f_{e_{\text{opt}}}^4 f_{t_{\text{opt}}}^4 \mu\psi + f_{e_{\text{opt}}}^4 f_{t_{\text{opt}}}^4 - 2f_{e_{\text{opt}}}^4 f_{t_{\text{opt}}}^2 \psi + f_{e_{\text{opt}}}^4 \psi^2 + f_{e_{\text{opt}}}^2 f_{t_{\text{opt}}}^6 \mu\mu_{k_{\text{opt}}} - 2f_{e_{\text{opt}}}^2 f_{t_{\text{opt}}}^4 \mu_{k_{\text{opt}}} - 2f_{e_{\text{opt}}}^2 f_{t_{\text{opt}}}^4 - 2f_{e_{\text{opt}}}^2 f_{t_{\text{opt}}}^2 \mu\psi^2 + 2f_{e_{\text{opt}}}^2 f_{t_{\text{opt}}}^2 \psi \\ &+ 4f_{e_{\text{opt}}}^2 f_{t_{\text{opt}}}^2 \psi - 2f_{e_{\text{opt}}}^2 \psi^2 + f_{t_{\text{opt}}}^4 \mu^2\psi^2 - 2f_{t_{\text{opt}}}^4 \mu\mu_{k_{\text{opt}}} \psi - f_{t_{\text{opt}}}^4 \mu\psi + f_{t_{\text{opt}}}^4 \mu_{k_{\text{opt}}}^2 + 2f_{t_{\text{opt}}}^4 \mu_{k_{\text{opt}}} + f_{t_{\text{opt}}}^4 + 2f_{t_{\text{opt}}}^2 \mu\psi^2 - 2f_{t_{\text{opt}}}^2 \mu_{k_{\text{opt}}} \psi \\ &- 2f_{t_{\text{opt}}}^2 \psi + \psi^2)/(4f_{e_{\text{opt}}}^2 f_{t_{\text{opt}}}^4 + 4\mu f_{e_{\text{opt}}}^2 f_{t_{\text{opt}}}^2 \psi^2 - 8f_{e_{\text{opt}}}^2 f_{t_{\text{opt}}}^2 \psi + 4f_{e_{\text{opt}}}^2 \psi^2))^{\frac{1}{2}}\end{aligned} \tag{19}$$

3.1.2 Ground Excitation. In this section, explicit expressions for the optimum parameters of the GERS-TMDI configuration subjected to the ground acceleration $\ddot{x}_g$ is presented.

The performance index of the system can be written as

$$PI = \frac{1}{2\pi}\int_{-\infty}^{\infty} \left|\frac{X_s(j\alpha)}{\ddot{X}_g(j\alpha)/\omega_s^2}\right|^2 d\alpha \tag{20}$$

The normalized transfer function is given as

$$\frac{X_s(j\alpha)}{\ddot{X}_g(j\alpha)/\omega_s^2} = \frac{B_4(j\alpha)^4 + B_3(j\alpha)^3 + B_2(j\alpha)^2 + B_1(j\alpha) + B_0}{A_6(j\alpha)^6 + A_5(j\alpha)^5 + A_4(j\alpha)^4 + A_3(j\alpha)^3 + A_2(j\alpha)^2 + A_1(j\alpha) + A_0} \tag{21}$$

where

$$\begin{cases} A_6 = \psi \\ A_5 = 2f_e\psi\zeta_e \\ A_4 = \psi + f_t^2\mu_k + f_e^2\psi + f_t^2 + f_t^2\mu\psi \\ A_3 = 2f_e\zeta_e(\psi + f_t^2 + f_t^2\mu\psi) \\ A_2 = f_t^2\mu_k + f_e^2\psi + f_t^2 + f_e^2f_t^2 + f_t^4\mu\mu_k + f_e^2f_t^2\mu\psi \\ A_1 = 2f_ef_t^2\zeta_e \\ A_0 = f_e^2f_t^2 \end{cases} \qquad \begin{cases} B_4 = \psi \\ B_3 = 2f_e\psi\zeta_e \\ B_2 = f_t^2\mu_k + f_e^2\psi + f_t^2 + f_t^2\mu\psi \\ B_1 = 2f_ef_t^2\zeta_e(\mu\psi + 1) \\ B_0 = f_e^2f_t^2(\mu\psi + 1) \end{cases} \tag{22}$$

Similar to the procedure described in Sec. 3.1.1, the final polynomial equations in terms of parameters f_t, μ and ψ can be obtained as

$$\begin{aligned}\psi(&f_t^4\mu^3\psi^2 + 2f_t^4\mu^2\psi + f_t^4\mu - 2f_t^2\mu\psi - 2f_t^2 + 2\psi)^2(2f_t^8\mu^5\psi^5 + 10f_t^8\mu^4\psi^4 + 20f_t^8\mu^3\psi^3 + 20f_t^8\mu^2\psi^2 + 10f_t^8\mu\psi + 2f_t^8 - 3f_t^6\mu^4\psi^5 \\ &- 13f_t^6\mu^3\psi^4 - 21f_t^6\mu^2\psi^3 - 15f_t^6\mu\psi^2 - 4f_t^6\psi + f_t^2\mu^3\psi^6 + 2f_t^2\mu^2\psi^5 + f_t^2\mu\psi^4 + 4f_t^2\psi^3 - 2\mu^2\psi^6 + 4\mu\psi^5 - 2\psi^4) = 0\end{aligned} \tag{23}$$

Solving Eq. (23) gives two sets of four optimum parameters. Each set can give a global or local minimum related to PI. The first set can be obtained by solving the expression in the first parenthesis of Eq. (23)

$$f_{t_{\text{opt}}} = \sqrt{\frac{\mu\psi + 1 - (\mu\psi + 1)r}{\mu(\mu\psi + 1)^2}} \tag{24}$$

$$f_{e_{\text{opt}}} = \sqrt{\frac{2\mu\psi + 2(\mu\psi + 1)r(1 - \mu\psi) + \mu^2\psi^2(3 - \mu^2\psi^2) - 2}{(\mu\psi + 1)r(2 - \mu^2\psi^2) + \mu^2\psi^2(4 + 3\mu\psi + \mu^2\psi^2) - 2}} \tag{25}$$

$$\mu_{k_{\text{opt}}} = \frac{2\mu^5\psi^5q^4((6 - \mu^2\psi^2 + 3\mu\psi)\mu\psi - 4) + 2\mu^5\psi^5q^3r((\mu^3\psi^3 + 4\mu^2\psi^2 + 5\mu\psi - 2)\mu\psi - 4)}{2\mu^4\psi^4q^4(\mu^3\psi^3 + 6\mu^2\psi^2 + 7\mu\psi - 4)} \tag{26}$$

$$\begin{aligned}\zeta_e = -((&64\mu\psi - 32qr + 112\mu^2\psi^2 - 184\mu^3\psi^3 - 194\mu^4\psi^4 + 156\mu^5\psi^5 + 163\mu^6\psi^6 - 27\mu^7\psi^7 - 48\mu^8\psi^8 - 6\mu^9\psi^9 + 3\mu^{10}\psi^{10} + \mu^{11}\psi^{11} \\ &+ 64\mu\psi qr + 64\mu^2\psi^2qr - 120\mu^3\psi^3qr - 70\mu^4\psi^4qr + 64\mu^5\psi^5qr + 36\mu^6\psi^6qr - 8\mu^7\psi^7qr - 6\mu^8\psi^8qr - 32)(2qr + 2q^3r^3 \\ &+ 15\mu^2\psi^2 + 9\mu^3\psi^3 - 10\mu^4\psi^4 - 10\mu^5\psi^5 - \mu^6\psi^6 + \mu^7\psi^7 + \mu\psi qr - \mu\psi q^3r^3 - 3\mu^2\psi^2qr - 4\mu^3\psi^3qr - \mu^4\psi^4qr \\ &+ \mu^5\psi^5qr - 4))/(2\mu^4\psi^4q^3(\mu\psi + 4)(\mu^2\psi^2 + 2\mu\psi - 1)^2(-\mu^3\psi^3 + 2\mu^2\psi^2 + \mu\psi - 4)^2)\end{aligned} \tag{27}$$

where

$$r = \sqrt{1 - 2\mu\psi} \tag{28a}$$

$$q = \mu\psi + 1 \tag{28b}$$

Solving the expression in the second parenthesis of Eq. (23) results in the second set of optimum parameters. The obtained expressions are lengthy; therefore, for the sake of brevity, only the optimum expressions (Eqs. (24)–(27)) are presented here and the accuracy of them will be checked using MATLAB optimization toolbox.

3.2 TE-ERS-TMDI-P Configuration. The governing equations of motion of the coupled system presented in Fig. 1(*b*) and subjected to force and ground excitations can be obtained as

$$m_s\ddot{x}_s + c_s\dot{x}_s + k_s x_s + k_T(x_s - x_T) + k_e(x_s - x_e) = -m_s\ddot{x}_g + F_w \tag{29a}$$

$$(m_T + b)\ddot{x}_T + k_T(x_T - x_s) + k_f I = -(m_T + b)\ddot{x}_g \tag{29b}$$

$$-k_f I + k_e(x_e - x_s) = 0 \tag{29c}$$

$$k_v(\dot{x}_e - \dot{x}_T) + RI + L\dot{I} + \frac{1}{C}\int I dt = 0 \tag{29d}$$

Applying Laplace transform into Eq. (29) and considering the primary structure undamped ($c_s = 0$), the equations of motion become

$$[(J\alpha)^2 + (1 + f_t^2\mu) + K_r]X_s - f_t^2\mu X_T - K_r X_e = \frac{F_w}{k_s} - \frac{\ddot{X}_g}{\omega_s^2} \tag{30a}$$

$$-f_t^2\mu X_s + [(J\alpha)^2\mu\psi + q_1 + f_t^2\mu]X_T - q_1 X_e = -\mu\psi\frac{\ddot{X}_g}{\omega_s^2} \tag{30b}$$

$$-K_r X_s - q_1 X_T + (K_r + q_1)X_e = 0 \tag{30c}$$

The electric current I can be written as follows:

$$I = \frac{k_s}{k_f} q_1 (X_T - X_e) \tag{31}$$

3.2.1 Force Excitation. Following the procedure described in the Sec. 3.1.1, the optimum parameters of f_T, f_e, μ_k, and ζ_e to minimize the vibrations of the primary structure (x_s) caused by the force excitation, F_w/K_s, can be obtained as follows:

$$PI = \frac{1}{2\pi}\int_{-\infty}^{\infty}\left|\frac{X_s(j\alpha)}{F_w/k_s}\right|^2 d\alpha \tag{32}$$

Here, PI is the performance index of the system and $(X_s(j\alpha)\, K_s)/F_w$ is the normalized transfer function

$$\frac{X_s(j\alpha)\, k_s}{F_w} = \frac{B_4(j\alpha)^4 + B_3(j\alpha)^3 + B_2(j\alpha)^2 + B_1(j\alpha) + B_0}{A_6(j\alpha)^6 + A_5(j\alpha)^5 + A_4(j\alpha)^4 + A_3(j\alpha)^3 + A_2(j\alpha)^2 + A_1(j\alpha) + A_0} \tag{33}$$

where

$$\left\{\begin{array}{c} A_6 = K_r\psi + f_t^2\mu\mu_k\psi \\ A_5 = 2K_r f_e\psi\zeta_e \\ A_4 = K_r f_t^2 + K_r\psi + K_r f_t^2\mu_k + K_r f_e^2\psi + f_t^4\mu\mu_k + f_t^2\mu\mu_k\psi + f_t^4\mu^2\mu_k\psi + K_r f_t^2\mu\psi + K_r f_t^2\mu\mu_k\psi \\ A_3 = 2K_r f_e\psi\zeta_e + 2K_r f_e f_t^2\mu\psi\zeta_e + 2K_r f_e f_t^2\zeta_e \\ A_2 = K_r f_t^2 + K_r f_t^2\mu_k + K_r f_e^2\psi + f_t^4\mu\mu_k + K_r f_e^2 f_t^2 + K_r f_e^2 f_t^2\mu\psi \\ A_1 = 2K_r f_e f_t^2\zeta_e \\ A_0 = K_r f_e^2 f_t^2 \end{array}\right. \qquad \left\{\begin{array}{c} B_4 = f_t^2\mu\mu_k\psi + K_r\psi \\ B_3 = 2K_r f_e\psi\zeta_e \\ B_2 = K_r f_t^2 + K_r f_t^2\mu_k + K_r f_e^2\psi + f_t^4\mu\mu_k \\ B_1 = 2K_r f_e f_t^2\zeta_e \\ B_0 = K_r f_e^2 f_t^2 \end{array}\right. \tag{34}$$

Applying the residue theorem [40] into Eq. (32), the PI can be obtained as

$$\begin{aligned} PI = (&K_r^2 f_e^4 f_t^4\mu^3\psi^3 + 3K_r^2 f_e^4 f_t^4\mu^2\psi^2 + 3K_r^2 f_e^4 f_t^4\mu\psi + K_r^2 f_e^4 f_t^4 - 2K_r^2 f_e^4 f_t^2\mu\psi^2 - 2K_r^2 f_e^4 f_t^2\psi + K_r^2 f_e^4\psi^2 - 2K_r^2 f_e^2 f_t^4\mu^2\mu_k\psi^2 + 4K_r^2 f_e^2 f_t^4\mu^2\psi^2\zeta_e^2 \\ &- 2K_r^2 f_e^2 f_t^4\mu^2\psi^2 - 4K_r^2 f_e^2 f_t^4\mu\mu_k\psi + 8K_r^2 f_e^2 f_t^4\mu\psi\zeta_e^2 - 4K_r^2 f_e^2 f_t^4\mu\psi - 2K_r^2 f_e^2 f_t^4\mu_k + 4K_r^2 f_e^2 f_t^4\zeta_e^2 - 2K_r^2 f_e^2 f_t^4 + K_r^2 f_e^2 f_t^2\mu\mu_k\psi^2 \\ &- 4K_r^2 f_e^2 f_t^2\mu\psi^2\zeta_e^2 + 2K_r^2 f_e^2 f_t^2\mu\psi^2 + 2K_r^2 f_e^2 f_t^2\mu_k\psi - 8K_r^2 f_e^2 f_t^2\psi\zeta_e^2 + 4K_r^2 f_e^2 f_t^2\psi + 4K_r^2 f_e^2\psi^2\zeta_e^2 - 2K_r^2 f_e^2\psi^2 + K_r^2 f_t^4\mu\mu_k^2\psi \\ &+ 2K_r^2 f_t^4\mu\mu_k\psi + K_r^2 f_t^4\mu\psi + K_r^2 f_t^4\mu_k^2 + 2K_r^2 f_t^4\mu_k + K_r^2 f_t^4 - 2K_r^2 f_t^2\mu_k\psi - 2K_r^2 f_t^2\psi + K_r^2\psi^2 - 2K_r f_e^2 f_t^6\mu^3\mu_k\psi^2 - 4K_r f_e^2 f_t^6\mu^2\mu_k\psi \\ &- 2K_r f_e^2 f_t^6\mu\mu_k + 2K_r f_e^2 f_t^4\mu^2\mu_k\psi^2 + 4K_r f_e^2 f_t^4\mu\mu_k\psi - 2K_r f_e^2 f_t^2\mu\mu_k\psi^2 + 2K_r f_t^6\mu^2\mu_k^2\psi + 2K_r f_t^6\mu^2\mu_k\psi + 2K_r f_t^6\mu\mu_k^2 + 2K_r f_t^6\mu\mu_k \\ &- 2K_r f_t^4\mu_k^2\psi - 4K_r f_t^4\mu\mu_k\psi + 2K_r f_t^2\mu\mu_k\psi^2 + f_t^8\mu^3\mu_k^2\psi + f_t^8\mu^2\mu_k^2 - 2f_t^6\mu^2\mu_k^2\psi + f_t^4\mu^2\mu_k^2\psi^2)/(4K_r^2 f_e f_t^2\mu\mu_k\psi^2\zeta_e) \end{aligned} \tag{35}$$

Similar to the procedure described in Sec. 3.1.1, the optimum parameters can be found as

$$f_{t_{\text{opt}}} = \frac{\sqrt{r - \mu\psi^2}}{2(\mu\psi + 1)} \tag{36}$$

$$f_{e_{\mathrm{opt}}} = \sqrt{\frac{K_r(\mu\psi + 1)(16\psi - 4r + \mu\psi(44\psi + 41\mu\psi^2 + 12\mu^2\psi^3 - 4\mu\psi r - 9r))}{4K_r(4\psi - r) + \mu\psi(-15K_r r + K_r\psi p + \mu^2\psi^2 h + \mu^3\psi^3 l)}} \tag{37}$$

$$\mu_{k_{\mathrm{opt}}} = -\frac{4K_r\mu^2\psi^2(r - \mu\psi^2)(\mu\psi + 1)^2}{(4K_r(4\psi - r) + \mu\psi(-15K_r r + K_r\psi p + \mu^2\psi^2 h + \mu^3\psi^3 l))} \tag{38}$$

$$\begin{aligned}
\zeta_{e_{\mathrm{opt}}} = {} & [(K_r^2(-3f_{e_{\mathrm{opt}}}^4 f_{t_{\mathrm{opt}}}^4\mu^3\psi^3 - 9f_{e_{\mathrm{opt}}}^4 f_{t_{\mathrm{opt}}}^4\mu^2\psi^2 - 9f_{e_{\mathrm{opt}}}^4 f_{t_{\mathrm{opt}}}^4\mu\psi - 3f_{e_{\mathrm{opt}}}^4 f_{t_{\mathrm{opt}}}^4 + 6f_{e_{\mathrm{opt}}}^2 f_{t_{\mathrm{opt}}}^2\mu\psi^2 + 6f_{e_{\mathrm{opt}}}^4 f_{t_{\mathrm{opt}}}^2\psi - 3f_{e_{\mathrm{opt}}}^4\psi^2 + 2f_{e_{\mathrm{opt}}}^2 f_{t_{\mathrm{opt}}}^4\mu^2\mu_{k_{\mathrm{opt}}}\psi^2 \\
& + 2f_{e_{\mathrm{opt}}}^2 f_{t_{\mathrm{opt}}}^4\mu^2\psi^2 + 4f_{e_{\mathrm{opt}}}^2 f_{t_{\mathrm{opt}}}^4\mu\mu_{k_{\mathrm{opt}}}\psi + 4f_{e_{\mathrm{opt}}}^2 f_{t_{\mathrm{opt}}}^4\mu\psi + 2f_{e_{\mathrm{opt}}}^2 f_{t_{\mathrm{opt}}}^4\mu_{k_{\mathrm{opt}}} + 2f_{e_{\mathrm{opt}}}^2 f_{t_{\mathrm{opt}}}^4 - f_{e_{\mathrm{opt}}}^2 f_{t_{\mathrm{opt}}}^2\mu\mu_{k_{\mathrm{opt}}}\psi^2 - 2f_{e_{\mathrm{opt}}}^2 f_{t_{\mathrm{opt}}}^2\mu\psi^2 - 2f_{e_{\mathrm{opt}}}^2 f_{t_{\mathrm{opt}}}^2\mu_{k_{\mathrm{opt}}}\psi \\
& - 4f_{e_{\mathrm{opt}}}^2 f_{t_{\mathrm{opt}}}^2\psi + 2f_{e_{\mathrm{opt}}}^2\psi^2 + f_{t_{\mathrm{opt}}}^4\mu\mu_{k_{\mathrm{opt}}}^2\psi + 2f_{t_{\mathrm{opt}}}^4\mu\mu_{k_{\mathrm{opt}}}\psi + f_{t_{\mathrm{opt}}}^4\mu\psi + f_{t_{\mathrm{opt}}}^4\mu_{k_{\mathrm{opt}}}^4 + 2f_{t_{\mathrm{opt}}}^4\mu_{k_{\mathrm{opt}}} + f_{t_{\mathrm{opt}}}^4 - 2f_{t_{\mathrm{opt}}}\mu_{k_{\mathrm{opt}}}\psi - 2f_{t_{\mathrm{opt}}}^2\psi + \psi^2) \\
& + K_r^2(2f_{e_{\mathrm{opt}}}^2 f_{t_{\mathrm{opt}}}^6\mu^3\mu_{k_{\mathrm{opt}}}\psi^2 + 4f_{e_{\mathrm{opt}}}^2 f_{t_{\mathrm{opt}}}^6\mu^2\mu_{k_{\mathrm{opt}}}\psi + 2f_{e_{\mathrm{opt}}}^2 f_{t_{\mathrm{opt}}}^6\mu\mu_{k_{\mathrm{opt}}} - 2f_{e_{\mathrm{opt}}}^2 f_{t_{\mathrm{opt}}}^4\mu^2\mu_{k_{\mathrm{opt}}}\psi^2 - 4f_{e_{\mathrm{opt}}}^2 f_{t_{\mathrm{opt}}}^4\mu\mu_{k_{\mathrm{opt}}}\psi + 2f_{e_{\mathrm{opt}}}^2 f_{t_{\mathrm{opt}}}^2\mu\mu_{k_{\mathrm{opt}}}\psi^2 \\
& + 2f_{t_{\mathrm{opt}}}^6\mu^2\mu_{k_{\mathrm{opt}}}^2\psi + 2f_{t_{\mathrm{opt}}}^6\mu^2\mu_{k_{\mathrm{opt}}}\psi + 2f_{t_{\mathrm{opt}}}^6\mu\mu_{k_{\mathrm{opt}}}^2 + 2f_{t_{\mathrm{opt}}}^6\mu\mu_{k_{\mathrm{opt}}} - 2f_{t_{\mathrm{opt}}}^4\mu\mu_{k_{\mathrm{opt}}}^2\psi - 4f_{t_{\mathrm{opt}}}^4\mu\mu_{k_{\mathrm{opt}}}\psi + 2f_{t_{\mathrm{opt}}}^2\mu\mu_{k_{\mathrm{opt}}}\psi^2) + f_{t_{\mathrm{opt}}}^8\mu^3\mu_{k_{\mathrm{opt}}}^2\psi + f_{t_{\mathrm{opt}}}^8\mu^2\mu_{k_{\mathrm{opt}}}^2 \\
& - 2f_{t_{\mathrm{opt}}}^6\mu^2\mu_{k_{\mathrm{opt}}}^2\psi + f_{t_{\mathrm{opt}}}^4\mu^2\mu_{k_{\mathrm{opt}}}^2\psi^2)/(K_r^2(4f_{e_{\mathrm{opt}}}^2 f_{t_{\mathrm{opt}}}^4\mu^2\psi^2 + 8f_{e_{\mathrm{opt}}}^2 f_{t_{\mathrm{opt}}}^4\mu\psi + 4f_{e_{\mathrm{opt}}}^2 f_{t_{\mathrm{opt}}}^4 - 4f_{e_{\mathrm{opt}}}^2 f_{t_{\mathrm{opt}}}^2\mu\psi^2 - 8f_{e_{\mathrm{opt}}}^2 f_{t_{\mathrm{opt}}}^2\psi + 4K_r^2 f_{e_{\mathrm{opt}}}^2\psi^2))]^{1/2}
\end{aligned} \tag{39}$$

where

$$r = \sqrt{\psi^2(17\mu^2\psi^2 + 32\mu\psi + 16)} \tag{40a}$$

$$p = (68 - 18\mu r + 111\mu\psi) \tag{40b}$$

$$h = (-7K_r r + 16\psi + 82K_r\psi) \tag{40c}$$

$$l = (-2r + 32\psi + 23K_r\psi + 18\mu\psi^2) \tag{40d}$$

3.2.2 Ground Excitation. The normalized transfer function for the model under ground excitation can be written as

$$\frac{X_s(j\alpha)}{\ddot{X}_g(j\alpha)/\omega_s^2} = \frac{B_4(j\alpha)^4 + B_3(j\alpha)^3 + B_2(j\alpha)^2 + B_1(j\alpha) + B_0}{A_6(j\alpha)^6 + A_5(j\alpha)^5 + A_4(j\alpha)^4 + A_3(j\alpha)^3 + A_2(j\alpha)^2 + A_1(j\alpha) + A_0} \tag{41}$$

where

$$\begin{gathered}
\left\{\begin{array}{c}
A_6 = \psi(\mu\mu_k f_t^2 + K_r) \\
A_5 = 2K_r f_e\psi\zeta_e \\
A_4 = K_r\psi + K_r f_t^2 + f_t^4\mu\mu_k + K_r f_t^2\mu_k + K_r f_e^2\psi + K_r f_t^2\mu\psi + f_t^2\mu\mu_k\psi + f_t^4\mu^2\mu_k\psi + K_r f_t^2\mu\mu_k\psi \\
A_3 = 2K_r f_e\zeta_e(\psi + f_t^2 + f_t^2\mu\psi) \\
A_2 = K_r f_t^2 + f_t^4\mu\mu_k + K_r f_e^2 f_t^2 + K_r f_t^2\mu_k + K_r f_e^2\psi + K_r f_e^2 f_t^2\mu\psi \\
A_1 = 2K_r f_e f_t^2\zeta_e \\
A_0 = K_r f_e^2 f_t^2
\end{array}\right. \\
\left\{\begin{array}{c}
B_4 = \psi(\mu\mu_k f_t^2 + K_r) \\
B_3 = 2K_r f_e\psi\zeta_e \\
B_2 = K_r f_t^2 + f_t^4\mu\mu_k + K_r f_t^2\mu_k + K_r f_e^2\psi + K_r f_t^2\mu\psi + f_t^4\mu^2\mu_k\psi + K_r f_t^2\mu\mu_k\psi \\
B_1 = 2K_r f_e f_t^2\zeta_e(\mu\psi + 1) \\
B_0 = K_r f_e^2 f_t^2(\mu\psi + 1)
\end{array}\right.
\end{gathered} \tag{42}$$

Following the procedure described in Sec. 3.1.1, the optimum parameters for this case can be found as

$$f_{t_{\mathrm{opt}}} = \frac{(\mu\psi + 1)(-\psi(3\mu\psi - 4))^{\frac{1}{2}}}{2(\mu\psi + 1)^2} \tag{43}$$

$$\mu_{k_{\rm opt}}=-\frac{128K_r\mu\psi(\mu\psi+1)^2}{(3\mu\psi-4)(16K_r-32\mu^2\psi^2+22K_r\mu^2\psi^2+3K_r\mu^3\psi^3+35K_r\mu\psi)} \tag{44}$$

$$f_{e_{\rm opt}}=\sqrt{-\frac{K_r(\mu\psi+1)(9\mu\psi-16)}{16K_r-32\mu^2\psi^2+22K_r\mu^2\psi^2+3K_r\mu^3\psi^3+35K_r\mu\psi}} \tag{45}$$

$$\zeta_{e_{\rm opt}}=\sqrt{-\frac{192K_r\mu\psi(\mu\psi+1)^2}{(9\mu\psi-16)(16K_r-32\mu^2\psi^2+22K_r\mu^2\psi^2+3K_r\mu^3\psi^3+35K_r\mu\psi)}} \tag{46}$$

3.3 TE-ERS-TMDI-S Configuration. The equations of motion of the coupled system presented in Fig. 1(*c*) and subjected to force F_w in the Laplace domain can be obtained as

$$[(j\alpha)^2+(1+f_t^2\mu)]X_s-f_t^2\mu X_T=\frac{F_w}{K_s} \tag{47a}$$

$$-f_t^2\mu X_s+[(j\alpha)^2\mu+f_t^2\mu+q_1]X_T-q_1X_e=0 \tag{47b}$$

$$-q_1X_T+[\delta\mu(j\alpha)^2+q_1]X_e=0 \tag{47c}$$

The normalized transfer function is given as

$$\frac{X_s(j\alpha)\,K_s}{F_w}=\frac{B_4(j\alpha)^4+B_3(j\alpha)^3+B_2(j\alpha)^2+B_1(j\alpha)+B_0}{A_6(j\alpha)^6+A_5(j\alpha)^5+A_4(j\alpha)^4+A_3(j\alpha)^3+A_2(j\alpha)^2+A_1(j\alpha)+A_0} \tag{48}$$

where

$$\left\{\begin{array}{c} A_6=\delta \\ A_5=2\delta f_e\zeta_e \\ A_4=\delta+\delta f_e^2+\delta f_t^2+f_t^2\mu_k+\delta f_t^2\mu+\delta f_t^2\mu_k \\ A_3=2\delta f_e\zeta_e(f_t^2\mu+f_t^2+1) \\ A_2=\delta f_e^2+\delta f_t^2+f_t^2\mu_k+f_t^4\mu_k+f_t^4\mu\mu_k+\delta f_e^2f_t^2+\delta f_t^2\mu_k+\delta f_t^4\mu\mu_k+\delta f_e^2f_t^2\mu \\ A_1=2\delta f_e f_t^2\zeta_e \\ A_0=\delta f_e^2f_t^2+\mu_k f_t^4 \end{array}\right.$$
$$\left\{\begin{array}{c} B_4=\delta \\ B_3=2\delta f_e\zeta_e \\ B_2=\delta f_e^2+\delta f_t^2+f_t^2\mu_k+\delta f_t^2\mu_k \\ B_1=2\delta f_e f_t^2\zeta_e \\ B_0=\delta f_e^2f_t^2+\mu_k f_t^4 \end{array}\right. \tag{49}$$

The optimum parameters are found using the same procedure described above

$$f_{t_{\rm opt}}=\sqrt{-\frac{A^*}{2}} \tag{50}$$

where

$$r=\sqrt{-3\mu^3(68\mu^3+849\mu^2-3360\mu+256)} \tag{51a}$$

$$A=\left(\frac{r}{9g^2}-\frac{8h^3}{27g^3}-\frac{(3\mu+12)2h}{6g^2}-\frac{2}{g}\right)^{\frac{1}{3}} \tag{51b}$$

$$B=\mu(13\mu^3+\mu^2-143\mu+48) \tag{51c}$$

$$g=\mu^3-3\mu^2+\mu-4 \tag{51d}$$

$$h=-\mu^2+\mu+6 \tag{51e}$$

$$A^*=A+3^{\frac{1}{2}}\left(Ai-\frac{Bi}{9Ag^2}\right)+\frac{4h}{3g}+\frac{B}{9Ag^2} \tag{51f}$$

$$\mu_{k_{opt}}=\frac{4\mu^2A^*}{2\mu A^*+A^{*2}+4A^*+4} \tag{52}$$

$$f_{e_{\mathrm{opt}}} = \sqrt{-\frac{-2\delta(1-2f_{t_{\mathrm{opt}}}^2) - 2\delta f_{t_{\mathrm{opt}}}^4(1+\mu_{k_{\mathrm{opt}}}) + 2f_{t_{\mathrm{opt}}}^2\mu_{k_{\mathrm{opt}}}(1-2f_{t_{\mathrm{opt}}}^2) + 2f_{t_{\mathrm{opt}}}^6\mu_{k_{\mathrm{opt}}}(1+\mu) - 2\delta f_{t_{\mathrm{opt}}}^2(\mu+\mu_{k_{\mathrm{opt}}}) + \delta f_{t_{\mathrm{opt}}}^6\mu\mu_{k_{\mathrm{opt}}}}{2\delta(1-2f_{t_{\mathrm{opt}}}^2) + 2\delta f_{t_{\mathrm{opt}}}^4(1+\mu)}} \tag{53}$$

$$\begin{aligned}\zeta_{e_{\mathrm{opt}}} = [((&+4f_{t_{\mathrm{opt}}}^8\mu_{k_{\mathrm{opt}}}^2 - 8\delta f_{e_{\mathrm{opt}}}^2 f_{t_{\mathrm{opt}}}^6\mu_{k_{\mathrm{opt}}} - 12\delta^2 f_{e_{\mathrm{opt}}}^4 f_{t_{\mathrm{opt}}}^4)(1+\mu) + (4f_{t_{\mathrm{opt}}}^4\mu_{k_{\mathrm{opt}}}^2 + 8\delta^2 f_{e_{\mathrm{opt}}}^2 - 12\delta^2 f_{e_{\mathrm{opt}}}^4)(1-2f_{t_{\mathrm{opt}}}^2) + (8\delta^2 f_{e_{\mathrm{opt}}}^2 f_{t_{\mathrm{opt}}}^4 - 8\delta f_{t_{\mathrm{opt}}}^6\mu_{k_{\mathrm{opt}}})(1+\mu_{k_{\mathrm{opt}}})\\
&+ 8\delta^2 f_{e_{\mathrm{opt}}}^2 f_{t_{\mathrm{opt}}}^2(\mu-\mu_{k_{\mathrm{opt}}}) + 8\delta^2 f_{t_{\mathrm{opt}}}^4\mu_{k_{\mathrm{opt}}}(1-\mu) + 4\delta^2 f_{t_{\mathrm{opt}}}^4(1+\mu_{k_{\mathrm{opt}}}^2-\mu) - 8\delta^2 f_{t_{\mathrm{opt}}}^2(1-\mu_{k_{\mathrm{opt}}}+\mu) + 4\delta^2(1+f_{t_{\mathrm{opt}}}^4\mu^2 - f_{e_{\mathrm{opt}}}^2 f_{t_{\mathrm{opt}}}^6\mu\mu_{k_{\mathrm{opt}}})\\
&+ 4\delta f_{t_{\mathrm{opt}}}^8\mu\mu_{k_{\mathrm{opt}}}^2 - 8\delta f_{t_{\mathrm{opt}}}^4\mu_{k_{\mathrm{opt}}}(\mu-\mu_{k_{\mathrm{opt}}}) + (16\delta f_{t_{\mathrm{opt}}}^4\mu_{k_{\mathrm{opt}}} - 8\delta f_{t_{\mathrm{opt}}}^2\mu_{k_{\mathrm{opt}}})(1+f_{e_{\mathrm{opt}}}^2)/(16\delta^2 f_{e_{\mathrm{opt}}}^2(1-2f_{t_{\mathrm{opt}}}^2) + 16\delta^2 f_{e_{\mathrm{opt}}}^2 f_{t_{\mathrm{opt}}}^2(f_{t_{\mathrm{opt}}}^2+\mu))]^{0.5}\end{aligned} \tag{54}$$

The explicit expression for the optimum parameters under ground excitation for this case are cumbersome; therefore, they are not shown here for the sake of brevity. However, we will present the results of this case using numerical analysis.

4 Numerical Analysis

The first part of the numerical simulation is to validate the obtained closed-form expressions of optimum vibration mitigation and energy harvesting. This is conducted using MATLAB optimization toolbox for mass and inertance ratios $\mu = 0.02$ and $\delta = 1$, respectively. The results are shown in Tables 2–6 and show excellent agreement with a maximum error of 0.09%.

Using the obtained optimum parameters, Figs. 3–6 compare the performance of all four configurations in terms of both vibration mitigation and energy harvesting by showing plots of the displacement of the primary structure and harvested powers. Figures 3 and 4 pertain to force (F_w) excitation and Figs. 5 and 6 are for ground ($\ddot{x}_g$) excitation. The results in these figures all show similar trends. In that, GERS-TMDI performs the best in terms of both vibration mitigation and energy harvesting, whereas the TE-ERS-TMDI-S performs the worst. The TE-ERS-TMDI-P and ERS-TMDI [36,38,39] show very similar performance in terms of vibration mitigation and energy harvesting. The percentage difference in performance between the GERS-TMDI and the TE-ERS-TMDI-S is about 25% for both ground and force excitations. The peak value of the normalized displacement for GERS-TMDI is reduced by around 2% in comparison with that of ERS-TMDI-P and ERS-TMDI configurations. The results also suggest that ERS-TMDI and TE-ERS-TMDI-P have almost the same performance for both ground and force excitations. Since GERS-TMDI configuration has the best performance and for the sake of brevity, the remainder of the numerical analysis is devoted to the understanding of the influence of some of the design variables on the performance of the novel energy-harvesting-vibration-absorber (i.e., GERS-TMDI configuration).

The three-dimensional plots depicted in Fig. 7 show the role of mass and inertance ratio on four optimum parameters for the case of the underground excitation. It can be observed that the mechanical tuning coefficient (f_t) decreases with increasing mass ratio, and it increases with increasing inertance ratio. The electrical tuning ratio (f_e) decreases with increasing both mass and inertance ratios. The results also show that the electromagnetic mechanical coupling (μ_k) and electrical damping ratios (ζ_e) increase with increasing both mass and inertance ratios.

For a better understanding of the role of the mass and inertance ratios on the optimal parameters, two-dimensional graphs are presented in Figs. 8 and 9. The results indicate that as the mass ratio increases, the effect of the inertance ratio becomes more significant on the electromagnetic mechanical coupling coefficient, electrical damping ratio, and electrical tuning ratio, whereas the effect of the inertance ratio on the mechanical tuning ratio remains constant. The results also indicate that the effect of mass ratio on the mechanical tuning ratio (f_t) is less significant than that of the inertance ratio. However, the effect of the mass ratio on the other three optimum parameters (f_e, μ_k, ζ_e) is more pronounced than that of the inertance ratio on f_e, μ_k, ζ_e.

Figure 10 depicts the normalized displacement of the primary structure under ground excitation. The results show that normalized displacement decreases with increasing inertance ratio δ. Figure 11 also indicates that the harvested power increases with increasing inertance ratio. These two observations are similar to those obtained for the ERS-TMDI configurations addressed in Refs. [35,36]. Figures 12–19 compare the performance of the parallel and series RLC circuit in terms of vibration mitigation and

Table 2 Designed parameters presented for the GERS-TMDI configurations with mass ratio $\mu = 0.02$ and inertance ratio $\delta = 1$ by analytical and numerical methods under force excitation (F_w)

Analytical optimum expressions	Example $\delta = 1$ and $\mu = 0.02$	
	Analytical	Numerical
$f_{t_{\mathrm{opt}}} = \sqrt{-\frac{A^*}{2}}$	$f_{t_{\mathrm{opt}}} = 1.455$	$f_{t_{\mathrm{opt}}} = 1.455$
$f_{e_{\mathrm{opt}}} = \sqrt{-\frac{f_{t_{\mathrm{opt}}}^4\mu^2\psi^2 - f_{t_{\mathrm{opt}}}^4\mu\psi + f_{t_{\mathrm{opt}}}^4 - 2f_{t_{\mathrm{opt}}}^2\psi + \psi^2}{-f_{t_{\mathrm{opt}}}^4 + \mu f_{t_{\mathrm{opt}}}^2\psi^2 + 2f_{t_{\mathrm{opt}}}^2\psi - \psi^2}}$	$f_{e_{\mathrm{opt}}} = 1.008$	$f_{e_{\mathrm{opt}}} = 1.008$
$\mu_{k_{\mathrm{opt}}} = -\frac{2\mu f_{e_{\mathrm{opt}}}^2 f_{t_{\mathrm{opt}}}^4\psi + 2f_{e_{\mathrm{opt}}}^2 f_{t_{\mathrm{opt}}}^4 - 4f_{e_{\mathrm{opt}}}^2 f_{t_{\mathrm{opt}}}^2\psi + 2f_{e_{\mathrm{opt}}}^2\psi^2 - 2f_{t_{\mathrm{opt}}}^4 - 2\mu f_{t_{\mathrm{opt}}}^2\psi^2 + 4f_{t_{\mathrm{opt}}}^2\psi - 2\psi^2}{\mu f_{t_{\mathrm{opt}}}^6 - 2f_{t_{\mathrm{opt}}}^4 + 2\psi f_{t_{\mathrm{opt}}}^2}$	$\mu_{k_{\mathrm{opt}}} = 0.087$	$\mu_{k_{\mathrm{opt}}} = 0.087$
$\zeta_{e_{\mathrm{opt}}} = ((f_{e_{\mathrm{opt}}}^4 f_{t_{\mathrm{opt}}}^4\mu\psi + f_{e_{\mathrm{opt}}}^4 f_{t_{\mathrm{opt}}}^4 - 2f_{e_{\mathrm{opt}}}^4 f_{t_{\mathrm{opt}}}^2\psi + f_{e_{\mathrm{opt}}}^4\psi^2 + f_{e_{\mathrm{opt}}}^2 f_{t_{\mathrm{opt}}}^6\mu\mu_{k_{\mathrm{opt}}} - 2f_{e_{\mathrm{opt}}}^2 f_{t_{\mathrm{opt}}}^4\mu_{k_{\mathrm{opt}}} - 2f_{e_{\mathrm{opt}}}^2 f_{t_{\mathrm{opt}}}^4 - 2f_{e_{\mathrm{opt}}}^2 f_{t_{\mathrm{opt}}}^2\mu\psi^2 + 2f_{e_{\mathrm{opt}}}^2 f_{t_{\mathrm{opt}}}^2\psi + 4f_{e_{\mathrm{opt}}}^2 f_{t_{\mathrm{opt}}}^2\psi - 2f_{e_{\mathrm{opt}}}^2\psi^2 + f_{t_{\mathrm{opt}}}^4\mu^2\psi^2 - 2f_{t_{\mathrm{opt}}}^4\mu\mu_{k_{\mathrm{opt}}}\psi - f_{t_{\mathrm{opt}}}^4\mu\psi + f_{t_{\mathrm{opt}}}^4\mu_{k_{\mathrm{opt}}}^2 + 2f_{t_{\mathrm{opt}}}^4\mu_{k_{\mathrm{opt}}} + f_{t_{\mathrm{opt}}}^4 + 2f_{t_{\mathrm{opt}}}^2\mu\psi^2 - 2f_{t_{\mathrm{opt}}}^2\mu_{k_{\mathrm{opt}}}\psi - 2f_{t_{\mathrm{opt}}}^2\psi + \psi^2)/(4f_{e_{\mathrm{opt}}}^2 f_{t_{\mathrm{opt}}}^4 + 4\mu f_{e_{\mathrm{opt}}}^2 f_{t_{\mathrm{opt}}}^2\psi^2 - 8f_{e_{\mathrm{opt}}}^2 f_{t_{\mathrm{opt}}}^2\psi + 4f_{e_{\mathrm{opt}}}^2\psi^2))^{1/2}$	$\zeta_{e_{\mathrm{opt}}} = 0.188$	$\zeta_{e_{\mathrm{opt}}} = 0.188$

Table 3 Designed parameters presented for the GERS-TMDI configurations with mass ratio $\mu = 0.02$ and inertance ratio $\delta = 1$ by analytical and numerical methods under ground excitation ($\ddot{x}_g$)

Analytical optimum expressions	Example $\delta = 1$ and $\mu = 0.02$	
	Analytical	Numerical
$f_{t_{opt}} = \sqrt{\frac{\mu\psi + 1 - (\mu\psi + 1)r}{\mu(\mu\psi + 1)^2}}$	$f_{t_{opt}} = 1.401$	$f_{t_{opt}} = 1.408$
$f_{e_{opt}} = \sqrt{\frac{2\mu\psi + 2(\mu\psi + 1)r(1 - \mu\psi) + \mu^2\psi^2(3 - \mu^2\psi^2) - 2}{(\mu\psi + 1)r(2 - \mu^2\psi^2) + \mu^2\psi^2(4 + 3\mu\psi + \mu^2\psi^2) - 2}}$	$f_{e_{opt}} = 0.971$	$f_{e_{opt}} = 0.976$
$\mu_{k_{opt}} = \frac{2\mu^5\psi^5 q^4((6 - \mu^2\psi^2 + 3\mu\psi)\mu\psi - 4) + 2\mu^5\psi^5 q^3 r((\mu^3\psi^3 + 4\mu^2\psi^2 + 5\mu\psi - 2)\mu\psi - 4)}{2\mu^4\psi^4 q^4(\mu^3\psi^3 + 6\mu^2\psi^2 + 7\mu\psi - 4)}$	$\mu_{k_{opt}} = 0.080$	$\mu_{k_{opt}} = 0.082$
$\zeta_{e_{opt}} = -((64\mu\psi - 32qr + 112\mu^2\psi^2 - 184\mu^3\psi^3 - 194\mu^4\psi^4 + 156\mu^5\psi^5 + 163\mu^6\psi^6 - 27\mu^7\psi^7 - 48\mu^8\psi^8 - 6\mu^9\psi^9 + 3\mu^{10}\psi^{10} + \mu^{11}\psi^{11} + 64\mu\psi qr + 64\mu^2\psi^2 qr - 120\mu^3\psi^3 qr - 70\mu^4\psi^4 qr + 64\mu^5\psi^5 qr + 36\mu^6\psi^6 qr - 8\mu^7\psi^7 qr - 6\mu^8\psi^8 qr - 32)(2qr + 2q^3r^3 + 15\mu^2\psi^2 + 9\mu^3\psi^3 - 10\mu^4\psi^4 - 10\mu^5\psi^5 - \mu^6\psi^6 + \mu^7\psi^7 + \mu\psi qr - \mu\psi q^3r^3 - 3\mu^2\psi^2 qr - 4\mu^3\psi^3 qr - \mu^4\psi^4 qr + \mu^5\psi^5 qr - 4))/(2\mu^4\psi^4 q^3(\mu\psi + 4)(\mu^2\psi^2 + 2\mu\psi - 1)^2(-\mu^3\psi^3 + 2\mu^2\psi^2 + \mu\psi - 4)^2)$	$\zeta_{e_{opt}} = 0.180$	$\zeta_{e_{opt}} = 0.183$

Table 4 Designed parameters presented for the TE-ERS-TMDI-P configurations with mass ratio $\mu = 0.02$ and inertance ratio $\delta = 1$ by analytical and numerical methods under force excitation (F_w)

Analytical optimum expressions	Example $\delta = 1$, $\mu = 0.02$, and $K_r = 0.2$	
	Analytical	Numerical
$f_{t_{opt}} = \frac{\sqrt{r - \mu\psi^2}}{2(\mu\psi + 1)}$	$f_{t_{opt}} = 1.339$	$f_{t_{opt}} = 1.339$
$f_{e_{opt}} = \sqrt{\frac{K_r(\mu\psi + 1)(16\psi - 4r + \mu\psi(44\psi + 41\mu\psi^2 + 12\mu^2\psi^3 - 4\mu\psi r - 9r))}{4K_r(4\psi - r) + \mu\psi(-15K_r r + K_r\psi p + \mu^2\psi^2 h + \mu^3\psi^3 l)}}$	$f_{e_{opt}} = 0.973$	$f_{e_{opt}} = 0.973$
$\mu_{k_{opt}} = -\frac{4K_r\mu^2\psi^2(r - \mu\psi^2)(\mu\psi + 1)^2}{(4K_r(4\psi - r) + \mu\psi(-15K_r r + K_r\psi p + \mu^2\psi^2 h + \mu^3\psi^3 l))}$	$\mu_{k_{opt}} = 0.082$	$\mu_{k_{opt}} = 0.082$
$\zeta_{e_{opt}} = [(K_r^2(-3f_{e_{opt}}^4 f_{t_{opt}}^4\mu^3\psi^3 - 9f_{e_{opt}}^4 f_{t_{opt}}^4\mu^2\psi^2 - 9f_{e_{opt}}^4 f_{t_{opt}}^4\mu\psi - 3f_{e_{opt}}^4 f_{t_{opt}}^4 + 6f_{e_{opt}}^2 f_{t_{opt}}^2\mu\psi^2 + 6f_{e_{opt}}^4 f_{t_{opt}}^2\psi - 3f_{e_{opt}}^4\psi^2 + 2f_{e_{opt}}^2 f_{t_{opt}}^4\mu^2\mu_{k_{opt}}\psi^2 + 2f_{e_{opt}}^2 f_{t_{opt}}^4\mu^2\psi^2 + 4f_{e_{opt}}^2 f_{t_{opt}}^4\mu\mu_{k_{opt}}\psi + 4f_{e_{opt}}^2 f_{t_{opt}}^4\mu\psi + 2f_{e_{opt}}^2 f_{t_{opt}}^4\mu_{k_{opt}} + 2f_{e_{opt}}^2 f_{t_{opt}}^4 - f_{e_{opt}}^2 f_{t_{opt}}^2\mu\mu_{k_{opt}}\psi^2 - 2f_{e_{opt}}^2 f_{t_{opt}}^2\mu\psi^2 - 2f_{e_{opt}}^2 f_{t_{opt}}^2\mu_{k_{opt}}\psi - 4f_{e_{opt}}^2 f_{t_{opt}}^2\psi + 2f_{e_{opt}}^2\psi^2 + f_{t_{opt}}^4\mu\mu_{k_{opt}}^2\psi + 2f_{t_{opt}}^4\mu\mu_{k_{opt}}\psi + f_{t_{opt}}^4\mu\psi + f_{t_{opt}}^4\mu_{k_{opt}}^4 + 2f_{t_{opt}}^4\mu_{k_{opt}} + f_{t_{opt}}^4 - 2f_{t_{opt}}\mu_{k_{opt}}\psi - 2f_{t_{opt}}^2\psi + \psi^2) + K_r^2(2f_{e_{opt}}^2 f_{t_{opt}}^6\mu^3\mu_{k_{opt}}\psi^2 + 4f_{e_{opt}}^2 f_{t_{opt}}^6\mu^2\mu_{k_{opt}}\psi + 2f_{e_{opt}}^2 f_{t_{opt}}^6\mu\mu_{k_{opt}} - 2f_{e_{opt}}^2 f_{t_{opt}}^4\mu^2\mu_{k_{opt}}\psi^2 - 4f_{e_{opt}}^2 f_{t_{opt}}^4\mu\mu_{k_{opt}}\psi + 2f_{e_{opt}}^2 f_{t_{opt}}^2\mu\mu_{k_{opt}}\psi^2 + 2f_{t_{opt}}^6\mu^2\mu_{k_{opt}}^2\psi + 2f_{t_{opt}}^6\mu^2\mu_{k_{opt}}\psi + 2f_{t_{opt}}^6\mu\mu_{k_{opt}}^2 + 2f_{t_{opt}}^6\mu\mu_{k_{opt}} - 2f_{t_{opt}}^4\mu\mu_{k_{opt}}^2\psi - 4f_{t_{opt}}^4\mu\mu_{k_{opt}}\psi + 2f_{t_{opt}}^2\mu\mu_{k_{opt}}\psi^2) + f_{t_{opt}}^8\mu^3\mu_{k_{opt}}^2\psi + f_{t_{opt}}^8\mu^2\mu_{k_{opt}}^2 - 2f_{t_{opt}}^6\mu^2\mu_{k_{opt}}^2\psi + f_{t_{opt}}^4\mu^2\mu_{k_{opt}}^2\psi^2)/(K_r^2(4f_{e_{opt}}^2 f_{t_{opt}}^4\mu^2\psi^2 + 8f_{e_{opt}}^2 f_{t_{opt}}^4\mu\psi + 4f_{e_{opt}}^2 f_{t_{opt}}^4 - 4f_{e_{opt}}^2 f_{t_{opt}}^2\mu\psi^2 - 8f_{e_{opt}}^2 f_{t_{opt}}^2\psi + 4K_r^2 f_{e_{opt}}^2\psi^2))]^{1/2}$	$\zeta_{e_{opt}} = 0.176$	$\zeta_{e_{opt}} = 0.176$

Table 5 Designed parameters presented for the TE-ERS-TMDI-P configurations with mass ratio $\mu = 0.02$ and inertance ratio $\delta = 1$ by analytical and numerical methods under ground excitation ($\ddot{x}_g$)

Analytical optimum expressions	Example $\delta = 1$, $\mu = 0.02$, and $K_r = 0.2$	
	Analytical	Numerical
$f_{t_{opt}} = \frac{(\mu\psi + 1)(-\psi(3\mu\psi - 4))^{\frac{1}{2}}}{2(\mu\psi + 1)^2}$	$f_{t_{opt}} = 1.380$	$f_{t_{opt}} = 1.380$
$\mu_{k_{opt}} = -\frac{128K_r\mu\psi(\mu\psi + 1)^2}{(3\mu\psi - 4)(16K_r - 32\mu^2\psi^2 + 22K_r\mu^2\psi^2 + 3K_r\mu^3\psi^3 + 35K_r\mu\psi)}$	$f_{e_{opt}} = 1.003$	$f_{e_{opt}} = 1.003$
$f_{e_{opt}} = \sqrt{-\frac{K_r(\mu\psi + 1)(9\mu\psi - 16)}{16K_r - 32\mu^2\psi^2 + 22K_r\mu^2\psi^2 + 3K_r\mu^3\psi^3 + 35K_r\mu\psi}}$	$\mu_{k_{opt}} = 0.081$	$\mu_{k_{opt}} = 0.081$
$\zeta_{e_{opt}} = \sqrt{-\frac{192K_r\mu\psi(\mu\psi + 1)^2}{(9\mu\psi - 16)(16K_r - 32\mu^2\psi^2 + 22K_r\mu^2\psi^2 + 3K_r\mu^3\psi^3 + 35K_r\mu\psi)}}$	$\zeta_{e_{opt}} = 0.175$	$\zeta_{e_{opt}} = 0.175$

Table 6 **Designed parameters presented for the TE-ERS-TMDI-S configurations with mass ratio $\mu = 0.02$ and inertance ratio $\delta = 1$ by analytical and numerical methods under force excitation (F_w)**

	Example $\delta = 1$ and $\mu = 0.02$	
Analytical optimum expressions	Analytical	Numerical
$f_{t_{\text{opt}}} = \sqrt{-\frac{A^*}{2}}$	$f_{t_{\text{opt}}} = 1.013$	$f_{t_{\text{opt}}} = 1.013$
$f_{e_{\text{opt}}} = \sqrt{-\frac{-2\delta(1-2f_{t_{\text{opt}}}^2) - 2\delta f_{t_{\text{opt}}}^4(1+\mu_{k_{\text{opt}}}) + f_{t_{\text{opt}}}^6 \mu_{k_{\text{opt}}}[2(1+\mu)+\delta\mu] - 2f_{t_{\text{opt}}}^2[\delta(\mu+\mu_{k_{\text{opt}}}) - \mu_{k_{\text{opt}}}(1-2f_{t_{\text{opt}}}^2)]}{2\delta(1-2f_{t_{\text{opt}}}^2) + 2\delta f_{t_{\text{opt}}}^4(1+\mu)}}$	$f_{e_{\text{opt}}} = 0.982$	$f_{e_{\text{opt}}} = 0.982$
$\mu_{k_{\text{opt}}} = \frac{4\mu^2 A^*}{2\mu A^* + A^{*2} + 4A^* + 4}$	$\mu_{k_{\text{opt}}} = 0.041$	$\mu_{k_{\text{opt}}} = 0.041$
$\zeta_{e_{\text{opt}}} = [((+4f_{t_{\text{opt}}}^8 \mu_{k_{\text{opt}}}^2 - 8\delta f_{e_{\text{opt}}}^2 f_{t_{\text{opt}}}^6 \mu_{k_{\text{opt}}} - 12\delta^2 f_{e_{\text{opt}}}^4 f_{t_{\text{opt}}}^4)(1+\mu) + (4f_{t_{\text{opt}}}^4 \mu_{k_{\text{opt}}}^2 + 8\delta^2 f_{e_{\text{opt}}}^2 - 12\delta^2 f_{e_{\text{opt}}}^4)(1-2f_{t_{\text{opt}}}^2) + (8\delta^2 f_{e_{\text{opt}}}^2 f_{t_{\text{opt}}}^4 - 8\delta f_{t_{\text{opt}}}^6 \mu_{k_{\text{opt}}})(1+\mu_{k_{\text{opt}}}) + 8\delta^2 f_{e_{\text{opt}}}^2 f_{t_{\text{opt}}}^2(\mu-\mu_{k_{\text{opt}}}) + 8\delta^2 f_{t_{\text{opt}}}^4 \mu_{k_{\text{opt}}}(1-\mu) + 4\delta^2 f_{t_{\text{opt}}}^4(1+\mu_{k_{\text{opt}}}^2-\mu) - 8\delta^2 f_{t_{\text{opt}}}^2(1-\mu_{k_{\text{opt}}}+\mu) + 4\delta^2(1+f_{t_{\text{opt}}}^4\mu^2 - f_{e_{\text{opt}}}^2 f_{t_{\text{opt}}}^6 \mu\mu_{k_{\text{opt}}}) + 4\delta f_{t_{\text{opt}}}^8 \mu\mu_{k_{\text{opt}}}^2 - 8\delta f_{t_{\text{opt}}}^4 \mu_{k_{\text{opt}}}(\mu-\mu_{k_{\text{opt}}}) + (16\delta f_{t_{\text{opt}}}^4 \mu_{k_{\text{opt}}} - 8\delta f_{t_{\text{opt}}}^2 \mu_{k_{\text{opt}}})(1+f_{e_{\text{opt}}}^2) / (16\delta^2 f_{e_{\text{opt}}}^2(1-2f_{t_{\text{opt}}}^2) + 16\delta^2 f_{e_{\text{opt}}}^2 f_{t_{\text{opt}}}^2(f_{t_{\text{opt}}}^2+\mu))]^{0.5}$	$\zeta_{e\text{opt}} = 0.041$	$\zeta_{e\text{opt}} = 0.041$

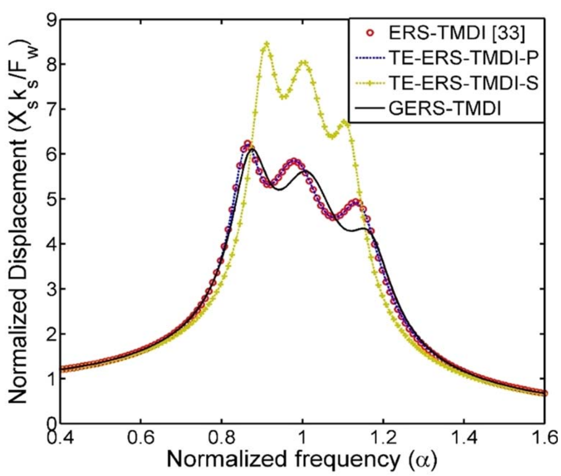

Fig. 3 Optimal frequency response under mass ratio $\mu = 0.02$ and inertance ratio $\delta = 1$ for vibration mitigation for the four different ERS-TMDI configurations under force excitation (F_w)

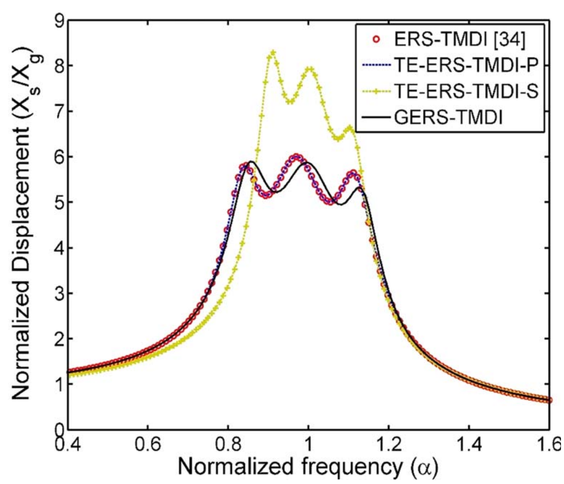

Fig. 5 Optimal frequency response under mass ratio $\mu = 0.02$ and inertance ratio $\delta = 1$ for vibration mitigation for the four different ERS-TMDI configurations under the ground excitation ($\ddot{x}_g$)

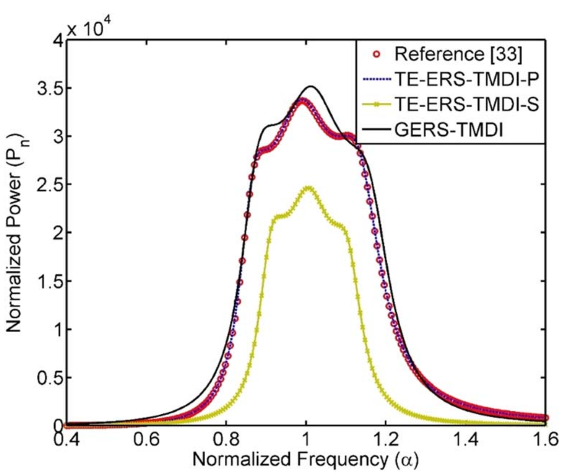

Fig. 4 Comparison of normalized power for the four ERS-TMDI configurations and with $\mu = 0.02$, $\delta = 1$, $k_v = 150$, $L = 1.17H$, and $R_e = 0.1\ \Omega$ under the force excitation (F_w)

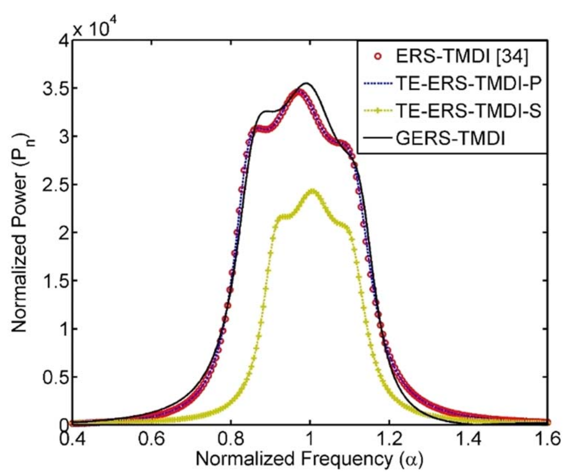

Fig. 6 Comparison of normalized power for different ERS-TMDI configurations and with $\mu = 0.02$, $\delta = 1$, $k_v = 150$, $L = 1.17H$, and $R_e = 0.1\ \Omega$ under the ground excitation ($\ddot{x}_g$)

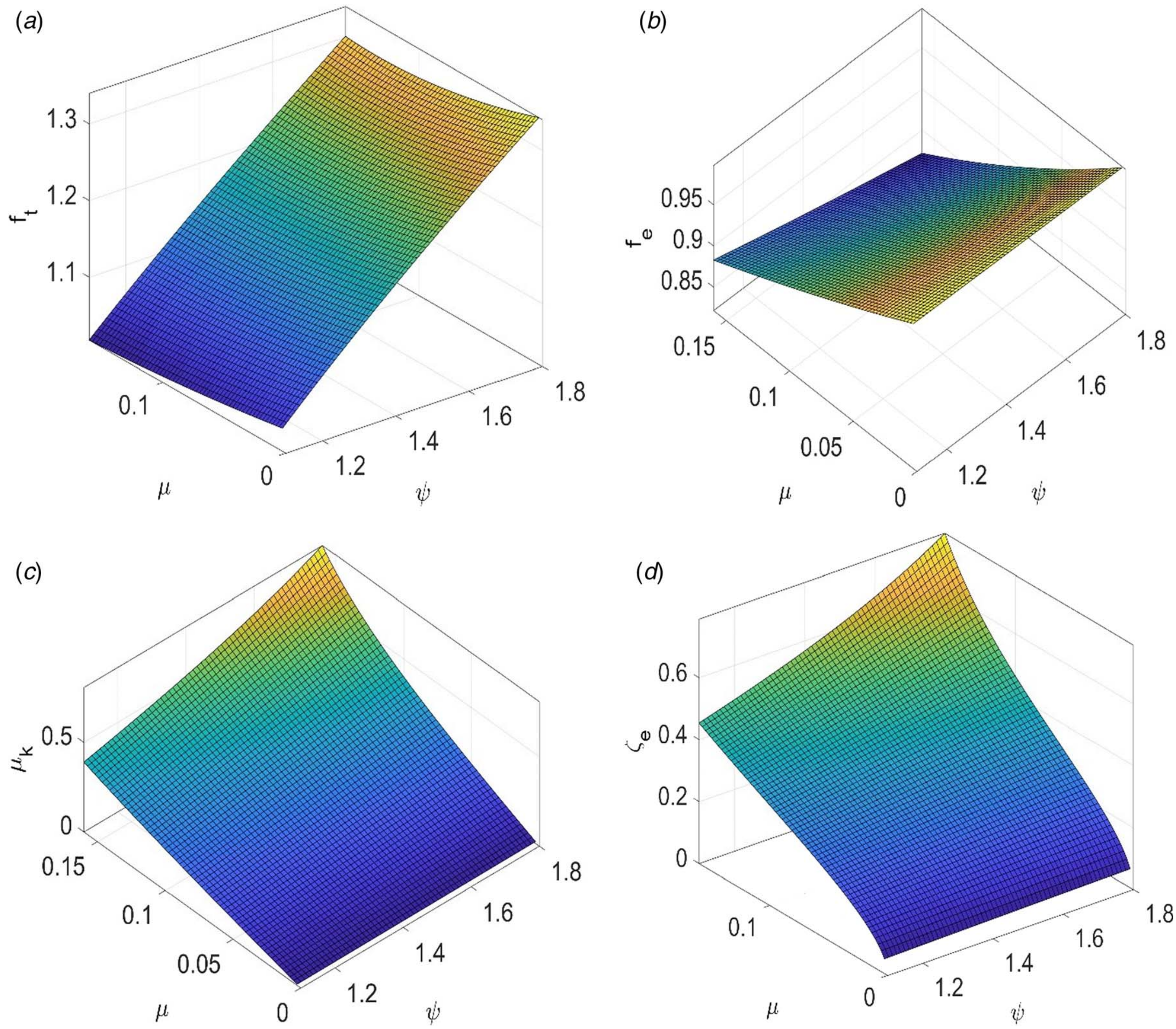

Fig. 7 Three-dimensional representation of variation of optimum parameters: (*a*) mechanical tuning ratio f_t, (*b*) electrical tuning ratio f_e, (c) electromagnetic mechanical coupling coefficient μ_k, and (*d*) electrical damping ratio ζ_e

energy harvesting for all four configurations under ground excitation. The details of the parallel RLC configuration formulations are given in the Appendix. We can observe that replacing the series RLC circuit with the parallel circuit improves the harvesting energy in all four configurations. The vibration mitigation performance, however, can improve or degrade depending on the configuration. For instance, Figs. 12 and 14 show a slight performance improvement with the GERS-TMDI and TE-ERS-TMDI-P configurations, respectively; whereas Figs. 16 and 18 show a slight performance deterioration with the TE-ERS-TMDI-S and ERS-TMDI configurations.

5 Conclusion

This paper presented three novel ERS-TMDI configurations and compares their performance to the conventional ERS-TMDI in terms of vibration mitigation and energy harvesting and under both force (wind) and ground (earthquake) excitations. Closed-form expressions for the optimal design parameters are obtained using H_2 norm criteria. The validation of the obtained explicit expressions is conducted using MATLAB optimization toolbox and showed excellent agreement. Comparison between the proposed configurations indicated that the novel GERS-TMDI performs the best, whereas, the TE-ERS-TMDI-S performs the worst in terms of both vibration mitigation and energy harvesting and under both wind and ground excitations. The TE-ERS-TMDI-P and the conventional ERS-TMDI showed similar performance. Parametric studies were carried out to examine the effect of mass and inertance ratios on the optimal design parameters of the GERS-TMDI. The results showed that increasing mass and inertance ratios both decrease the electrical tuning ratio. The effect of inertance ratio on the electrical tuning ratio, electromagnetic mechanical coupling coefficient, and electric damping ratio is more significant for higher mass ratios. These findings suggest that for systems with larger mass ratios, uncertainty in inerter ratio will have a larger effect on the electrical tuning ratio, the electromagnetic mechanical coupling coefficient, and the electric damping ratio. Parametric studies also showed that increasing the inertance ratio enhances the performance of GERS-TMDI in terms of both vibration mitigation and energy harvesting. Numerical examples also demonstrated that replacing the series RLC with a parallel circuit can improve the energy harvesting performance of all configurations. In terms of vibration mitigation,

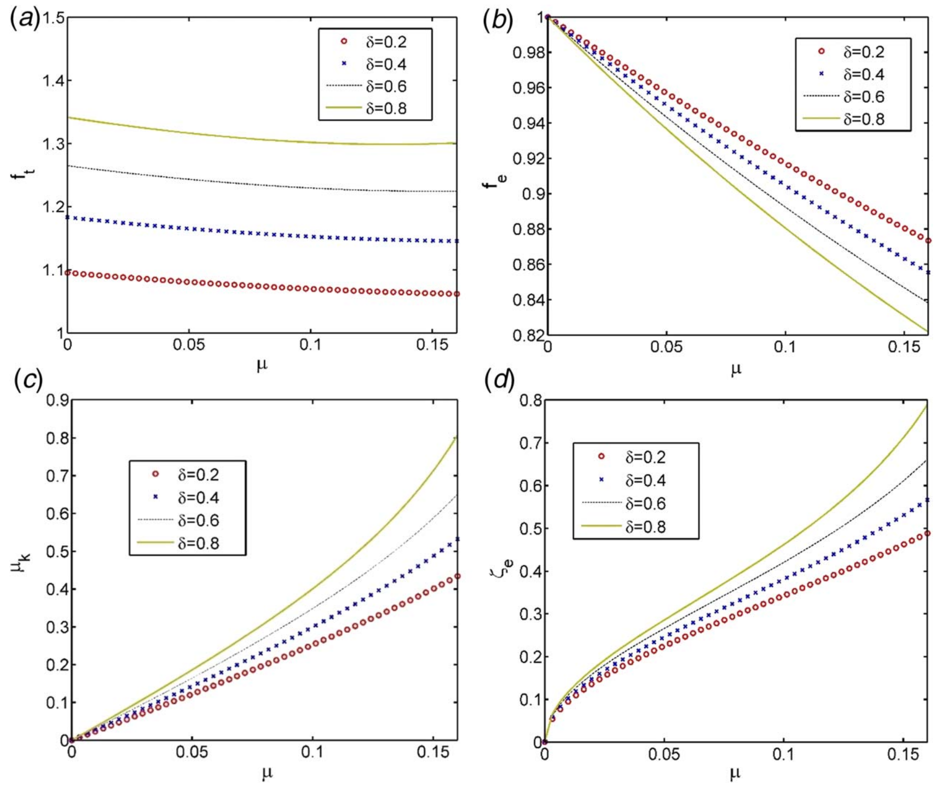

Fig. 8 Two-dimensional graphical representations of optimum parameters with respect to mass ratio: (*a*) mechanical tuning ratio f_t, (*b*) electrical tuning ratio f_e, (c) electromagnetic mechanical coupling coefficient μ_k, and (*d*) electrical damping ratio ζ_e

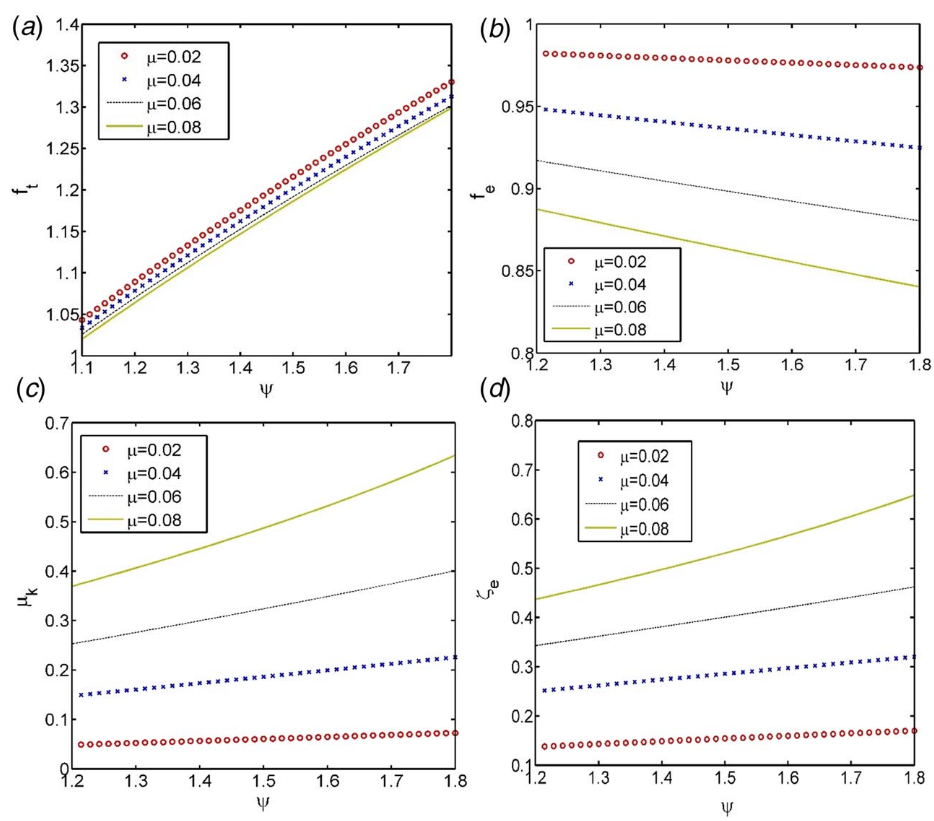

Fig. 9 Two-dimensional graphical representations of optimum parameters with respect to inertance ratio: (*a*) mechanical tuning ratio f_t, (*b*) electrical tuning ratio f_e, (c) electromagnetic mechanical coupling coefficient μ_k, and (*d*) electrical damping ratio ζ_e

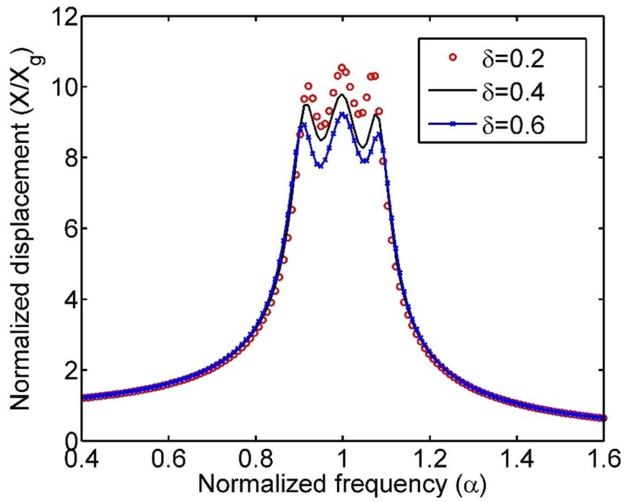

Fig. 10 Schematic of the optimal frequency response of the primary structure under mass ratio $\mu = 0.02$ and different inertance ratios for GERS-TMDI under ground excitation ($\ddot{x}_g$)

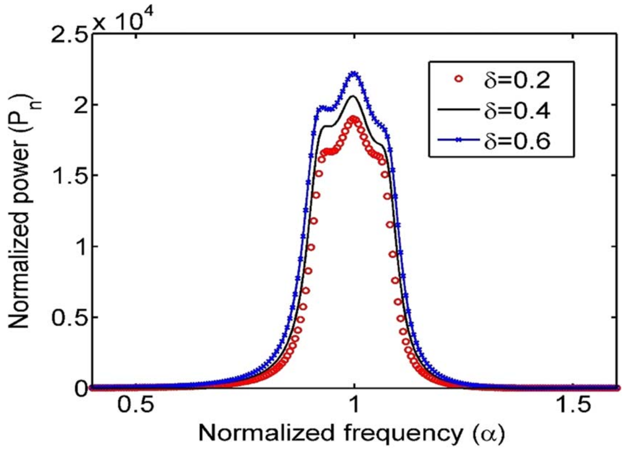

Fig. 11 Comparison of normalized power of the GERS-TMDI under different inertance ratios and with the mass ratio $\mu = 0.02$, $k_v = 150$, $L = 1.17H$, and $R_e = 0.1\ \Omega$ under ground excitation ($\ddot{x}_g$)

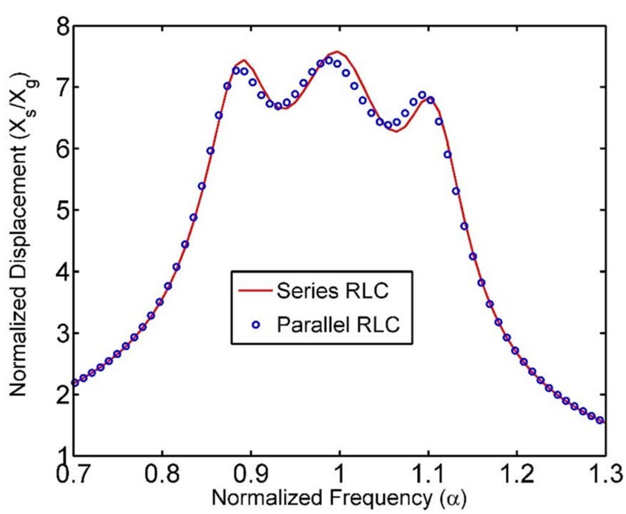

Fig. 12 Comparison of normalized deformation of primary structure with series and parallel RLC circuits using mass ratio $\mu = 0.02$ and inertance ratio $\delta = 0.2$ related to GERS-TMDI configuration under ground excitation ($\ddot{x}_g$)

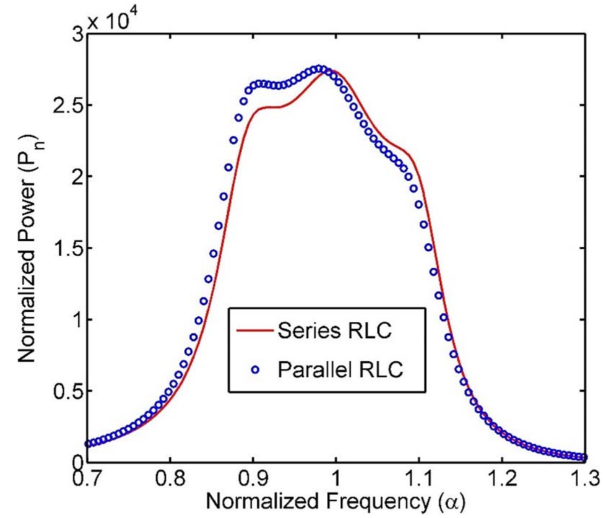

Fig. 13 Comparison of normalized power of GERS-TMDI for different RLC circuits using mass ratio $\mu = 0.02$ and inertance ratio $\delta = 0.2$ under ground excitation ($\ddot{x}_g$)

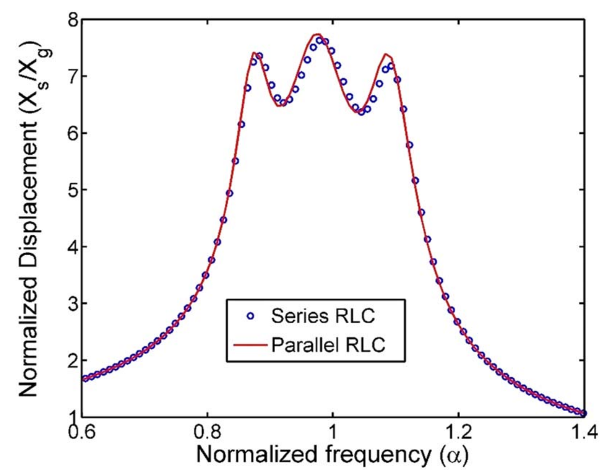

Fig. 14 Comparison of normalized displacement of primary structure with series and parallel RLC circuits using mass ratio $\mu = 0.02$ and inertance ratio $\delta = 0.2$ related to TE-ERS-TMDI-P configuration under ground excitation ($\ddot{x}_g$)

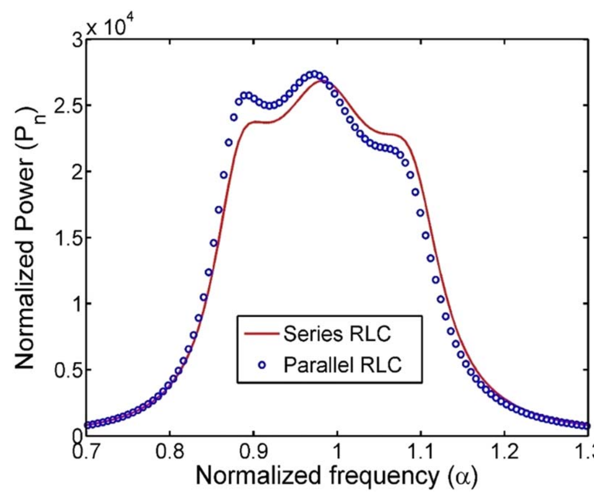

Fig. 15 Comparison of normalized power of TE-ERS-TMDI-P for different RLC circuits using mass ratio $\mu = 0.02$ and inertance ratio $\delta = 0.2$ under ground excitation ($\ddot{x}_g$)

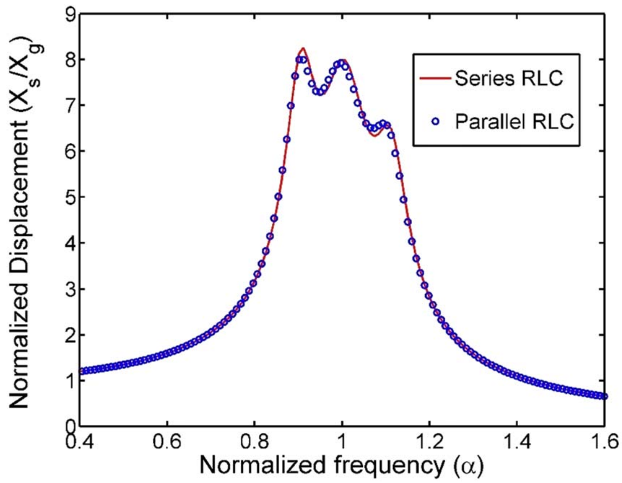

Fig. 16 Comparison of normalized displacement of primary structure with series and parallel RLC configurations using mass ratio $\mu = 0.02$ and inertance ratio $\delta = 0.2$ related to TE-ERS-TMDI-S configuration under ground excitation ($\ddot{x}_g$)

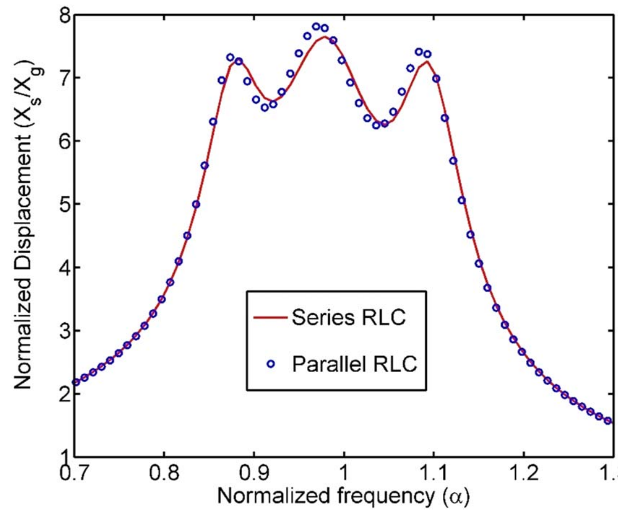

Fig. 18 Comparison of normalized displacement of primary structure with series and parallel RLC circuits using mass ratio $\mu = 0.02$ and inertance ratio $\delta = 0.2$ related to ERS-TMDI configuration under ground excitation ($\ddot{x}_g$)

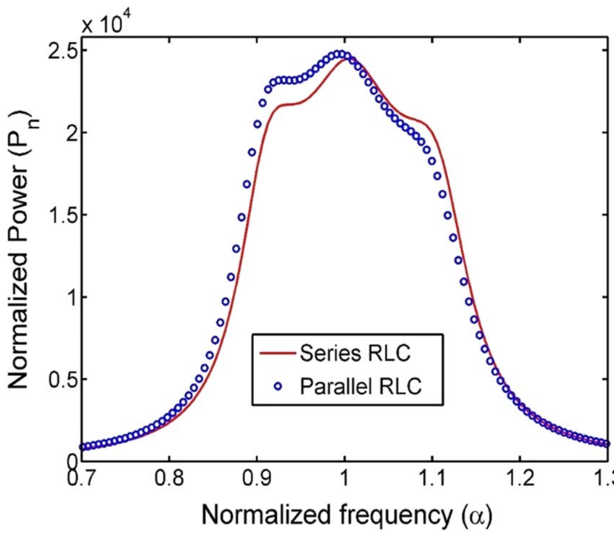

Fig. 17 Comparison of normalized power of TE-ERS-TMDI-S for different RLC circuits using mass ratio $\mu = 0.02$ and inertance ratio $\delta = 0.2$ under ground excitation ($\ddot{x}_g$)

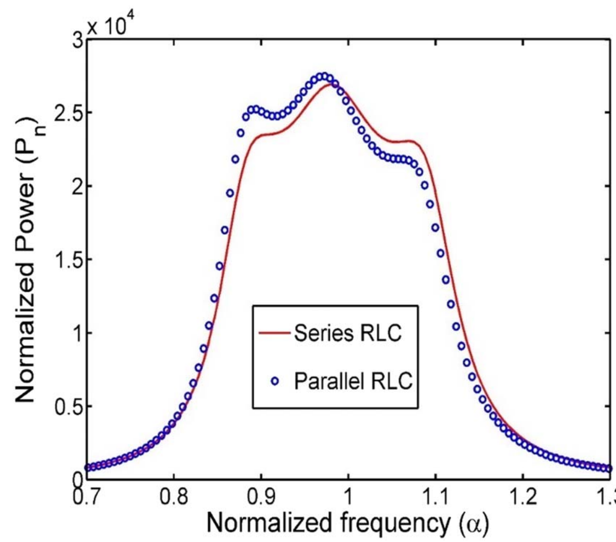

Fig. 19 Comparison of normalized power of ERS-TMDI configuration for different RLC circuits using mass ratio $\mu = 0.02$ and inertance ratio $\delta = 0.2$ under ground excitation ($\ddot{x}_g$)

however, it can degrade or improve the performance. All configurations, except the ERS-TMDI, exhibited local optimum solutions. Future work will focus on identifying global optimum solutions for all three configurations and experimentally validating the findings in this paper.

Appendix

The normalized equations of motion of GERS-TMDI configuration with parallel RLC circuit under the ground excitation are obtained as

$$[(j\alpha)^2 + (1 + f_t^2\mu)]X_s - f_t^2\mu X_T = -\frac{\ddot{X}_g}{\omega_s^2} \tag{A1}$$

$$(-f_t^2\mu)X_s + [\psi(j\alpha)^2\mu + f_t^2\mu + q_2]X_s = -\mu\psi\frac{\ddot{X}_g}{\omega_s^2} \tag{A2}$$

and

$$I = \frac{k_s}{k_f} q_2(X_T) \tag{A3}$$

where

$$q_2 = \frac{\mu_k f_T^2 \mu[(j\alpha)^3 + 2\zeta_e f_e (j\alpha)^2]}{2\zeta_e f_e (j\alpha)^2 + f_e^2 (j\alpha)^2 + 2\zeta_e f_e^3} \tag{A4}$$

The performance index of the system can be written as

$$PI = \frac{1}{2\pi}\int_{-\infty}^{\infty}\left|\frac{X_s(j\alpha)}{\ddot{X}_g(j\alpha)/\omega_s^2}\right|^2 d\alpha \tag{A5}$$

$$\frac{X_s(j\alpha)}{\ddot{X}_g(j\alpha)/\omega_s^2}=\frac{B_4(j\alpha)^4+B_3(j\alpha)^3+B_2(j\alpha)^2+B_1(j\alpha)+B_0}{A_6(j\alpha)^6+A_5(j\alpha)^5+A_4(j\alpha)^4+A_3(j\alpha)^3+A_2(j\alpha)^2+A_1(j\alpha)+A_0} \tag{A6}$$

where

$$\begin{cases} B_0=2f_e^3f_t^2\zeta_e+2f_e^3f_t^2\mu\psi\zeta_e \\ B_1=f_e^2f_t^2+f_e^2f_t^2\mu\psi \\ B_2=2f_ef_t^2\zeta_e+2f_e^3\psi\zeta_e+2f_ef_t^2\mu_k\zeta_e+2f_ef_t^2\mu\psi\zeta_e \\ B_3=f_t^2\mu_k+f_e^2\psi \\ B_4=2f_e\psi\zeta_e \end{cases}$$

$$\begin{cases} A_0=2f_e^3f_t^2\zeta_e \\ A_1=f_e^2f_t^2 \\ A_2=2f_e^3f_t^2\zeta_e+2f_ef_t^2\zeta_e+2f_e^3\psi\zeta_e+2f_ef_t^2\mu_k\zeta_e+2f_ef_t^4\mu\mu_k\zeta_e+2f_e^3f_t^2\mu\psi\zeta_e \\ A_3=f_t^2\mu_k+f_e^2\psi+f_e^2f_t^2+f_t^4\mu\mu_k+f_e^2f_t^2\mu\psi \\ A_4=2f_e\psi\zeta_e+2f_ef_t^2\zeta_e+2f_e^3\psi\zeta_e+2f_ef_t^2\mu_k\zeta_e+2f_ef_t^2\mu\psi\zeta_e \\ A_5=f_t^2\mu_k+f_e^2\psi \\ A_6=2f_e\psi\zeta_e \end{cases} \tag{A7}$$

Applying the residue theorem into Eq. (A4), the PI can be obtained as

$$\begin{aligned} PI=(&4f_e^6f_t^4\mu^4\psi^4\zeta_e^2+16f_e^6f_t^4\mu^3\psi^3\zeta_e^2+24f_e^6f_t^4\mu^2\psi^2\zeta_e^2+16f_e^6f_t^4\mu\psi\zeta_e^2+4f_e^6f_t^4\zeta_e^2+4f_e^6f_t^2\mu^3\psi^4\zeta_e^2-12f_e^6f_t^2\mu\psi^2\zeta_e^2-8f_e^6f_t^2\psi\zeta_e^2 \\ &+4f_e^6\psi^2\zeta_e^2+8f_e^4f_t^6\mu^4\mu_k\psi^3\zeta_e^2+24f_e^4f_t^6\mu^3\mu_k\psi^2\zeta_e^2+24f_e^4f_t^6\mu^2\mu_k\psi\zeta_e^2+8f_e^4f_t^6\mu\mu_k\zeta_e^2+8f_e^4f_t^4\mu^3\mu_k\psi^3\zeta_e^2-8f_e^4f_t^4\mu^3\psi^3\zeta_e^2 \\ &+f_e^4f_t^4\mu^3\psi^3-24f_e^4f_t^4\mu^2\psi^2\zeta_e^2+3f_e^4f_t^4\mu^2\psi^2-16f_e^4f_t^4\mu\mu_k\psi\zeta_e^2-24f_e^4f_t^4\mu\psi\zeta_e^2+3f_e^4f_t^4\mu\psi-8f_e^4f_t^4\mu_k\zeta_e^2-8f_e^4f_t^4\zeta_e^2+f_e^4f_t^4 \\ &+16f_e^4f_t^2\mu\psi^2\zeta_e^2-2f_e^4f_t^2\mu\psi^2+8f_e^4f_t^2\mu_k\psi\zeta_e^2+16f_e^4f_t^2\psi\zeta_e^2-2f_e^4f_t^2\psi-8f_e^4\psi^2\zeta_e^2+f_e^4\psi^2+4f_e^2f_t^8\mu^4\mu_k^2\psi^2\zeta_e^2+8f_e^2f_t^8\mu^3\mu_k^2\psi\zeta_e^2 \\ &+4f_e^2f_t^8\mu^2\mu_k^2\,\zeta_e^2+4f_e^2f_t^6\mu^3\mu_k^2\psi^2\zeta_e^2-4f_e^2f_t^6\mu^3\mu_k\psi^2\zeta_e^2+f_e^2f_t^6\mu^3\mu_k\psi^2-8f_e^2f_t^6\mu^2\mu_k\psi\zeta_e^2+2f_e^2f_t^6\mu^2\mu_k\psi-4f_e^2f_t^6\mu\mu_k^2\zeta_e^2-4f_e^2f_t^6\mu\mu_k\zeta_e^2 \\ &+f_e^2f_t^6\mu\mu_k+4f_e^2f_t^4\mu^2\psi^2\zeta_e^2+8f_e^2f_t^4\mu\mu_k\psi\zeta_e^2-2{*}f_e^2f_t^4\mu\mu_k\psi+8f_e^2f_t^4\mu\psi\zeta_e^2+4f_e^2f_t^4\mu_k^2\zeta_e^2+8f_e^2f_t^4\mu_k\zeta_e^2-2f_e^2f_t^4\mu_k+4f_e^2f_t^4\zeta_e^2 \\ &-4f_e^2f_t^2\mu\psi^2\zeta_e^2-8f_e^2f_t^2\mu_k\psi\zeta_e^2+2f_e^2f_t^2\mu_k\psi-8f_e^2f_t^2\psi\zeta_e^2+4f_e^2\psi^2\zeta_e^2+f_t^4\mu_k^2)/(4f_ef_t^6\mu\mu_k\zeta_e) \end{aligned} \tag{A8}$$

Numerical analysis was performed on the PI (A8) using MATLAB optimization toolbox.

References

[1] Frahm, H., 1911, "Device for Damping Vibrations of Bodies," U.S. Patent," 989,958, pp. 3576–3580.

[2] Den Hartog, J. P., 1956, *Mechanical Vibrations*, 4th ed., McGraw-Hill, New York.

[3] Salvi, J., and Rizzi, E., 2016, "Closed-Form Optimum Tuning Formulas for Passive Tuned Mass Dampers Under Benchmark Excitations," Smart Struct. Syst., **17**(2), pp. 231–256.

[4] Ormondroyd, J., and Hartog, J. P. D., 1928, "Theory of the Dynamic Vibration Absorber," ASME J. Appl. Mech., **50**(7), pp. 9–22.

[5] Brock, J. E., 1946, "A Note on the Damped Vibration Absorber," ASME J. Appl. Mech., **68**, p. A-284.

[6] Wang, F. C., Hong, M. F., and Lin, T. C., 2011, "Designing and Testing a Hydraulic Inerter," Proc. Inst. Mech. Eng., Part C, **225**(1), pp. 66–72.

[7] Wang, J.-F., and Lin, C.-C., 2015, "Extracting Parameters of TMD and Primary Structure From the Combined System Response," Smart Struct. Syst., **16**(5), pp. 937–960.

[8] Marian, L., and Giaralis, A., 2017, "The Tuned Mass-Damper-Inerter for Harmonic Vibrations Suppression, Attached Mass Reduction, and Energy Harvesting," Smart Struct. Syst., **19**(6), pp. 665–678.

[9] Ricciardelli, F., and Vickery, B. J., 1999, "Tuned Vibration Absorbers With Dry Friction Damping," Earthquake Eng. Struct. Dyn., **28**(7), pp. 707–724.

[10] Bukhari, M. A., and Barry, O. R., 2018, "Nonlinear Vibrations Analysis of Overhead Power Lines: A Beam With Mass–Spring–Damper–Mass Systems," ASME J. Vib. Acoust., **140**(3), p. 031004.

[11] Xu, K., and Igusa, T., 1992, "Dynamic Characteristics of Multiple Substructures With Closely Spaced Frequencies," Earthquake Eng. Struct. Dyn., **21**(12), pp. 1059–1070.

[12] Lin, C. C., Wang, J. F., and Chen, B. L., 2005, "Train-Induced Vibration Control of High-Speed Railway Bridges Equipped With Multiple Tuned Mass Dampers," ASCE J. Bride Eng., **10**(4), pp. 398–414.

[13] Casciati, F., and Giuliano, F., 2009, "Performance of Multi-TMD in the Towers of Suspension Bridges," J. Vib. Control, **15**(6), pp. 821–847.

[14] Zuo, L., 2009, "Effective and Robust Vibration Control Using Series Multiple Tuned-Mass Dampers," ASME J. Vib. Acoust., **131**(3), p. 031003.

[15] De Angelis, M., Perno, S., and Reggio, A., 2012, "Dynamic Response and Optimal Design of Structures With Large Mass Ratio TMD," Earthquake Eng. Struct. Dyn., **41**(1), pp. 41–60.

[16] Smith, M. C., 2002, "Synthesis of Mechanical Networks: The Inerter," IEEE Trans. Automat. Control, **47**(10), pp. 1648–1662.

[17] Marian, L., and Giaralis, A., 2014, "Optimal Design of a Novel Tuned Mass-Damper-Inerter (TMDI) Passive Vibration Control Configuration for Stochastically Support-Excited Structural Systems," Probab. Eng. Mech., **38**(Oct.), pp. 156–164.

[18] Smith, M. C., and Wang, F. U.-C., 2004, "Performance Benefits in Passive Vehicle Suspensions Employing Inerters," Veh. Syst. Dyn., **42**(4), pp. 235–257.

[19] Papageorgiou, C., and Smith, M. C., 2006, "Positive Real Synthesis Using Matrix Inequalities for Mechanical Networks: Application to Vehicle Suspension," IEEE Trans. Control Syst. Technol., **14**(3), pp. 423–435.

[20] Hu, Y. L., Chen, M. Z. Q., and Shu, Z., 2014, "Passive Vehicle Suspensions Employing Inerters With Multiple Performance Requirements," J. Sound Vib., **333**(8), pp. 2212–2225.

[21] Jiang, J. Z., Matamoros-Sanchez, A. Z., Goodall, R. M., and Smith, M. C., 2012, "Passive Suspensions Incorporating Inerters for Railway Vehicles," Veh. Syst. Dyn., **50**(1), pp. 263–276.

[22] Wang, F.-C., Liao, M.-K., Liao, B.-H., Su, W.-J., and Chan, H.-A., 2009, "The Performance Improvements of Train Suspension Systems With Mechanical Networks Employing Inerters," Veh. Syst. Dyn., **47**(7), pp. 805–830.

[23] Salvi, J., and Giaralis, A., 2016, "Concept Study of a Novel Energy Harvesting-Enabled Tuned Mass-Damper-Inerter (EH-TMDI) Device for Vibration Control of Harmonically-Excited Structures," J. Phys.: Conf. Ser., **744**(1), p. 012082.

[24] Giaralis, A., and Petrini, F., 2017, "Wind-Induced Vibration Mitigation in Tall Buildings Using the Tuned Mass Damper-Inerter (TMDI)," ASCE J. Struct. Eng., **143**(9), p. 04017127.

[25] Sun, H., Zuo, L., Wang, X., Peng, J., and Wang, W., 2019, "Exact H_2 Optimal Solution of the Inerter-Based Isolation System for Building Structures," Struct. Control Health Monit., **26**(6), p. e2357.

[26] Ikago, K., Saito, K., and Inoue, N., 2012, "Seismic Control of Single-Degree-of-Freedom Structure Using Tuned Viscous Mass Damper," Earthquake Eng. Struct. Dyn., **41**(3), pp. 453–474.

[27] Papageorgiou, C., and Smith, M. C., 2005, "Laboratory Experimental Testing of Inerters," Proceedings of the 44th IEEE Conference on Decision and Control, Seville, Spain, Dec. 15, pp. 3351–3356.

[28] Cheung, Y. L., and Wong, W. O., 2011, "H_2 Optimization of a None-Traditional Dynamic Vibration Absorber for Vibration Control of Structures Under Random Force Excitation," J. Sound Vib., **330**(6), pp. 1039–1044.

[29] Gonzalez-Buelga, A., Clare, L. R., Cammarano, A., Neild, S. A., Burrow, S. G., and Inman, D. J., 2014, "An Optimised Tuned Mass Damper/Harvester Device," Struct. Control Health Monit., **21**(8), pp. 1154–1169.

[30] Barry, O., and Bukhari, M., 2017, "On the Modeling and Analysis of an Energy Harvester Moving Vibration Absorber for Power Lines," ASME Dynamic Systems and Control Conference, Tysons Corner, VA, Oct. 11–13, p. V002T23A005.

[31] Liu, Y., 2016, "Design, Modeling and Control of Vibration Systems With Electromagnetic Energy Harvesters and Their Application to Vehicle Suspensions," Doctoral dissertation, Virginia Tech.

[32] Gonzalez-Buelga, A., Clare, L. R., Neild, S. A., Jiang, J. Z., and Inman, D. J., 2015, "An Electromagnetic Inerter-Based Vibration Suppression," Smart Mater. Struct., **24**(5), p. 055015.

[33] Scruggs, J., and Lindner, D. K., 1999, "Active Energy Control in Civil Structures. In Symposium on Smart Structures and Materials," Smart Struct. Mater., **3671**, pp. 194–205.

[34] Scruggs, J. T., and Iwan, W. D., 2003, "Control of a Civil Structure Using an Electric Machine With Semiactive Capability," ASCE J. Struct. Eng., **129**(7), pp. 951–959.

[35] Liu, Y., Lin, C.-C., Parker, J., and Zuo, L., 2016, "Exact H_2 Optimal Tuning and Experimental Verification of Energy-Harvesting Series Electromagnetic Tuned-Mass Dampers," ASME J. Vib. Acoust., **138**(6), p. 061003.

[36] Luo, Y., Sun, H., Wang, X., Zuo, L., and Chen, C., 2017, "Wind Induced Vibration Control and Energy Harvesting of Electromagnetic Resonant Shunt Tuned Mass-Damper-Inerter for Building Structures," Shock Vib., pp. 1–13.

[37] Javidialesaadi, A., and Wierschem, N. E., 2018, "Three-Element Vibration Absorber–Inerter for Passive Control of Single-Degree-of-Freedom Structures," ASME J. Vib. Acoust., **140**(6), p. 061007.

[38] Farzaneh Joubaneh, E., Barry, O. R., and Zuo, L., 2018, "On the Vibration Suppression and Energy Harvesting of Building Structures Using an Electromagnetic-Inerter-Absorber," ASME Dynamic Systems and Control Conference, ASME Paper No. V002T18A005.

[39] Sun, H., Luo, Y., Wang, X., and Zuo, L., 2017, "Seismic Control of a SDOF Structure Through Electromagnetic Resonant Shunt Tuned Mass-Damper-Inerter and Exact H_2 Optimal Solution," J. Vibroeng., **19**(3), pp. 2063–2079.

[40] Gradshteyn, I. S., and Ryzhik, I. M., 1980, *Table of Integrals Series and Product*, Academic Press, New York.